Semi-passive trailing-edge flaps

For ultimate and fatigue load reductions on wind turbines

J. N. La Porte

Technische Universiteit Delft

TU Delft

Semi-passive trailing-edge flaps

For ultimate and fatigue load reductions on wind turbines

by

J. N. La Porte

to obtain the degree of Master of Science
at Delft University of Technology
and
at Danmarks Tekniske Universitet

Student number (TUD):	4176219	
Student number (DTU):	s173600	
Project duration:	November 1, 2018 – August 1, 2019	
Thesis committee:	Dr. ir. T. K. Barlas,	DTU, supervisor
	Prof. H. A. Madsen,	DTU, supervisor
	Prof. Dr. ir. C. S. Ferreira,	TU Delft, supervisor
	Prof. Dr. ir. J. W. van Wingerden,	TU Delft, supervisor

An electronic version of this thesis is available at `http://repository.tudelft.nl/`.

DTU

EWEM

TU Delft

Contents

Summary

Semi-passive trailing edge flaps for ultimate and fatigue load reductions on wind turbines by J N La Porte

THIS thesis investigates the application of a semi-passive trailing edge flap system with the goal of reducing fatigue and ultimate loads on wind turbine blades. The research is done in HAWC2 on the DTU 10MW reference turbine. Firstly, a literature study is conducted on the state of the art of 'smart' rotors, resulting in a clear formulation of research questions and an outline of research process. Building on prior work of a passive flap which changes the camber of the airfoil in reaction to blade vibrations, a new semi-passive design is proposed which actively changes the pre-load of the spring at the flap hinge. The passive part consists of an offset mass connected to the trailing edge flap which is free to move inside the blade structure. The added active component allows to control the mean of the flap deflection oscillation increasing the effectiveness of the system. Five parameters of the flap are varied including: span, chord, hinge spring stiffness, offset mass and the distance of the offset mass to the hinge.
A preliminary study was done in a low-fidelity model made in MATLAB which tests the flap model with input based on statistics gathered from the baseline turbine. Without aeroelastic response of the turbine these calculations are fast and many combinations of the five parameters are investigated. The result of this study is many sets of parameters that show high load alleviating potential.
After converting the MATLAB model into a `.dll` that can connect to HAWC2 to obtain dynamic inputs and includes aeroelastic response, the resulting parameter sets from the low fidelity model were tested. Results were then analyzed in terms of their lifetime and ultimate loads on the blades and tower and the effect on the AEP.
The results yield significant lifetime reductions in the blade root flap-wise direction. The edgewise lifetime loads were increased due to the added mass in the blade. Likewise the torsion moment at the blade root increases which is an added effect caused by the pitching moment of a flap. AEP is not significantly influenced, however, tower top loads decrease but tower bottom loads show an increase. This more robust passive design achieves 75% of the blade root flap-wise reductions that a similar active flap reaches.
Further research should be done on increasing the turbine size and optimizing the turbine in combination with the load alleviation method. This will give insight in how much the cost of energy can be reduced. Furthermore, the pre-load control must be integrated in the current control system.

Nomenclature

α	Angle of attack
$\ddot{\delta}$	Flap acceleration
ΔL	The change in lift of the flap compared to the baseline
δ	Flap angle
$\dot{\delta}$	Flap velocity
ν	Kinematic viscosity
ϕ	Rotation of the actuator driving the pre-load
ρ	Density of air
a	Power law exponent
a_H	Acceleration of the blade at the hinge in c2def orientation
a_{mb}	Acceleration at the hinge in the blade root coordinate system
a_{om}	Acceleration of the ofset mass in the blade section coordinate system
C	Total rotation matrix for Euler Type I angles
c	Blade sectional chord
c_f	Flap chord
C_H	Hinge moment coefficient
Cl_b	Lift coefficient of the baseline model
Cl_f	Lift coefficient of the model with flap
d_{om}	1D distance of the offset mass to the hinge
F	Force acting on the blade in fig. 2.3
f	1P frequency of rotor rotation
i	Index per load range
J_f	Inertia of the flap and offset mass
K_f	Spring stiffness of the hinge
m	Slope of the Wöhler curve
M_a	Aerodynamic moment of the flap around the hinge
M_i	Inertial moment of the flap around the hinge
M_p	Moment due to the preload of the spring at the flap hinge
m_{om}	Mass of the offset mass
$M_{p,new}$	Preload of a new case with different parameters

$M_{p,old}$	Preload of an already tuned case
n	Current time-step
N_i	Amount of cycles per load range i
$N_{eq,L}$	The lifetime of a wind turbine, approximated as 1E7
N_{eq}	The total simulation time of a signal in seconds
P	The probability of a certain event
q	Dynamic Pressure
R	The blade length
r	Dimensionless radial position along the blade
R_x	Rotation matrix around x-axis
R_y	Rotation matrix around y-axis
R_z	Rotation matrix around z-axis
r_{om}	2D distance between offset mass and hinge
S_f	Spanwise length of the flap
S_i	The amplitude of the load range
$stel$	Short term equivalent load
t	Total simulation time
u_0	Wind speed at the reference height
u_{ref}	Reference wind speed for Weibull distribution of the wind
V_{rel}	Inflow velocity relative to the blade section
z_0	Reference height of the wind speed for the power law
dlc	Design load case
step	The step taken between wind speeds from cut in to cut out
wdir	Abbreviation of wind direction
Weight	The resulting weight that is given to each wind speed and direction in the dlc
wsp	Abreviation of wind speed

Preface

MUCH can happen over the course of 9 months and it is amazing how time can fly in the meanwhile. This two year journey as an EWEM student was priceless in terms of personal development and knowledge acquired. It was also emotional at times as you make friends each semester and are forced to say goodbye or farewell multiple times.

At the start of my thesis, I was set on combining mechanical engineering with aerodynamic rotor design representing my bachelor and master. After a couple of e-mails, I soon came in contact with four people who would all do their part in supervising my thesis. With your enthusiasm and sometimes a nudge in the right direction, I ended up with a most interesting topic. During the last 9 months some moments were more difficult than others but overall I enjoyed doing research and contributing an ever so small part. In Isaac Newton's words: *"If I have seen further it is by standing on ye shoulders of Giants."*, I could not be more thankful to my supervisors. Carlos Simao Ferreira, for your time and critical feedback. Helge A. Madsen for sharing your experience during our meetings. Jan-Willem van Wingerden for playing a key role in choosing the topic. And of course, Thanasis Barlas, for guiding me through this process and inspiring me in our weekly meetings. I enjoyed working together with you all.

To my dear friends from EWEM Erin, Simone, Patrick, Gert-Jan, Rogier, Reinier, Dylan and Federico, I wish you the best in the coming years. To all of my roommates in H1: you guys are ... amazing man. I would like to thank my 'friendship' in Denmark: DTU Exiles Rugby for providing an outlet, a family and good memories. We will meet again. Of course, mom and dad, where would I be without you? Thank you for always being there for me and giving me advice. Lastly, I would like to thank my girlfriend, Elise, for supporting me and her encouragement these last months.

1 Introduction

WIND energy is making great technological leaps, driven by the stimulus of staying competitive to fossil fuel solutions and climate goals set by the government. In Europe, wind energy accounts for 18% of the total installed power generation capacity [1]. This drive to continue installing more Giga Watts of clean energy however, is subject to much competition. Photo-voltaics are swiftly decreasing their prices. Hydro-power still contributes the highest percentage of modern renewable energy [2], despite their questionable effect on creatures in the water. Therefore, it is important to continue improving our renewable energy sources. This chapter will briefly introduce the topic's motivation, research questions and outline of the thesis.

1.1. Motivation to increase turbine size

Wind energy relies on converting the kinetic energy from wind to electricity, without emitting harmful substances. To remain competitive, the cost of energy (CoE) must be as low as possible. This figure relates the costs of the entire turbine including production, placement and maintenance to the revenue from the energy it is able to sell over its lifetime. Reducing the CoE is key to staying competitive on the market and can, among others, be achieved by:

- Reducing the cost of required equipment
- Maximizing the produced energy
- Reducing operation and maintenance costs
- Accurate prediction of lifetime

Increasing the size of the turbine can increase power production and consequently reduce the amount of turbines necessary for the same amount of power production. Fewer turbines per area means fewer components in need of maintenance and fewer foundations which are costly when placed offshore. With improved and more complex structural design, blade size have increased over the years. Just short of 20 years ago turbines started exceeding the 1MW rating with rotor diameters of 50m. Ten years ago the Enercon E-126 blade diameter exceeded the wingspan of a Boeing 838. This summer, 2019, GE is testing its Haliade-X with 12-14MW rated power on the Maasvlakte in Rotterdam. The rotor diameter will be the largest in the world at 220m and its height is just 64m short of the Eiffel Tower. Continuing this growth becomes increasingly challenging following the square-cube law [3]. This law states that the swept area of the rotor increases squared and the volume, thus the blade mass, increases cubed. In the words of Galileo Galilei (1638) *'... the ratio of volumes is larger than the ratio of surfaces'* [4]. In other words, the mass of the blade increases faster than the area that is gained by it, resulting in structural design difficulties.

1.2. The 'smart' rotor concept

With size limits being reached, 'smart' rotor solutions are being developed which allow the rotor to adapt to their aerodynamic circumstances [5]. The ultimate goal of a 'smart' rotor is to reduce the loads on the blade to

allow longer blades or extend their lifetime. Control is being used to adapt the pitch of individual blades when necessary [6], something that was once deemed too sophisticated for wind turbine applications. Translating tabs, that influence blade aerodynamics, have also been explored as a smart concept [7]. Another solution is the use of trailing edge flaps, with the purpose of increasing Annual Energy Production (AEP) or reducing fatigue and ultimate loads [8]. Blade fatigue is quantified by the amount of cycles that have occurred at a load range in the turbines lifetime. The flap-wise movement of the blade occurs out of the rotor plane and is, among others, due to turbulence creating a velocity gradient changing with height. Structural properties as pre-bend, coning and tilt also add to the out of plane movement of the blade. Reducing fatigue loads, targets minimizing the amount of cycles and the range of flap-wise load fluctuations. Reducing ultimate loads can often be achieved by the same trailing edge flap as for fatigue loads. In the literature review in chapter 2, load alleviation techniques will be evaluated thoroughly.

1.3. Objective of this thesis

The goal of this research is to demonstrate the feasibility of an inertial-driven semi-passive flap, which changes the aerodynamic behavior of the blade by reacting to blade vibrations. The pre-load of the passive flap will be controlled by an active element reducing ultimate and fatigue loads while minimizing AEP loss.

1.4. Outline of this thesis

The thesis will achieve the above mentioned objective in the following chapters:

- **Chapter 2** presents a review of the available literature on state of the art load alleviation techniques and a clear formulation of research (sub-)questions.
- **Chapter 3** presents the methodology used in this research and contains the derivation of the equations of motion, an explanation of the aeroelastic code HAWC2 and theory it is built on.
- **Chapter 4** presents and analyses the results of a low fidelity model. This model relies on statistics of the inflow conditions experienced on the DTU 10MW reference turbine. The goal of this simulation is to evaluate different designs and combination of design parameters.
- **Chapter 5** presents the results and analysis of high-fidelity simulation using HAWC2. These simulations include aeroelastic analysis of the system. The results compare loads and power for the cases with and without the semi-passive solution.
- **Chapter 6** reflects on the course of the thesis and summarizes the results with respect to the research questions.

2

Literature Review of load alleviation methods for wind turbines

In this chapter the concept of load alleviation techniques for wind turbines is discussed. As mentioned before, load alleviation can be lumped into two major categories: active and passive load alleviation methods. These methods will be discussed sequentially and will be reviewed from their origins in aerospace until their application in state of the art wind turbine technology. Following, a review will be done on theory and numbers relevant to the topic of this thesis.

2.1. Active load alleviation methods

Active load alleviation relies on real time measurements of a certain quantity related to wind turbine loads. This could be, for instance, wind speeds measured at hub height or loads measured at the blade root. Conventional wind turbines, as the DTU 10MW [9] and the NREL 5MW [10] wind turbine, commonly use pitch control where all blades pitch collectively to track rated power in the full load region. Observer based control, without need of wind speed measurements, which minimizes the squared error has demonstrated closed loop convergence on the NREL 5MW turbine in research done by Corradini et al. [11]. This form of pitch control relies on accurate measurements and regulation of blade pitch and generator torque on the turbine. Rotational speed is regulated by adjusting the generator torque. The goal of this control method is, however, not to exceed the maximum generator torque while reducing the flap-wise loads on the blade to stay within the design constraints.

2.1.1. Individual pitch control

Directly related to collective pitch control, is individual pitch control (IPC), which controls the pitch of the individual blades relying on their azimuthal position. This shows a decrease in fatigue loads of 20%-30% at the blade root and 30%-40% at the hub according to Bossanyi [12]. The maximum out of plane loads are almost cancelled out at the dominant 1P frequency of rotating components. The reduction of the tower loads are dictated by the 3P frequency that is unaffected by the use of IPC. This method has also proved to work on the basis of local inflow measurements on a blade section in research done by Thomsen et al. [13]. The measurements were successfully used to predict the local inflow over the entire blade. All of the IPC methods show large reductions between 10% and 20% but, result in added wear of the pitching mechanism due to increased speed of pitching.

2.1.2. Active flaps

Active flaps are currently being greatly explored and have originated from a rigid trailing-edge flap known from aircraft, which required flaps already from their first flights. Differences are, however, that wind turbine blades may not consist of metals or contain electrical components. In wind turbines the technology is only recently being researched which commenced with Shape Memory Alloys (SMA). This morphing geometry concept realizes a continuous deformation of the trailing-edge and has already proved to be promising in preliminary studies coupling blade root forces to the flap via active control conduced by Barlas et al. [14]. The smooth change in geometry requires elastic materials which are subject to fatigue. Research was continued to

design a mechanism that acts by means of a pressurized fluid which dramatically simplifies the structure and makes actuating servo-motors in the wing redundant according to Madsen [15]. The concept can be made without electrical components in the blade and can react to blade vibrations or moments, by adding a bit of complexity. Other rigid trailing-edge flaps have been inspected and are called discrete trailing-edge flaps. The downside to the discrete flaps is that the components of the mechanism can be subject to abrasion and start corroding. The discontinuous change in camber can reduce the lift to drag ratio but does simplify the mechanical design and possibly increase robustness. Recent studies by Oltmann [16] have shown that a cyclic motion of the active flap can eliminate the cyclic variation of the blade root bending moment. These simulations were run on German Aerospace Center's in-house rotor simulation code S4 for the IWT-7.5MW. The result of this research is very applicable to any form of trailing-edge flap in terms of flap deflection amplitude and phase shift of the cyclic motion.

2.2. Passive load alleviation methods

Passive solutions have the benefit that they need no control element to achieve load alleviation over the rotor blade. This also comes with the downside that they are only active in a select region making the passive device inherently limited. Still, passive solutions are interesting in terms of their simplicity and reliability, which could reduce the price and operation and maintenance costs with respect to active solutions. Several passive solutions have been proposed over the years and can be lumped into two major categories: full span solutions and sectional solutions.

2.2.1. Full span aeroelastic tailoring (AT)

This type of load alleviation relies on a coupled deformation of the blade which ensures that a flap-wise deformation results in aerodynamic conditions which reduces loads according to Carrolo [17]. Several combinations have been explored combining bend twist coupling (BTC), flap edge coupling and others. This coupling can be achieved through altering the blade geometry or smart engineering of the materials in the blade. The latter has recently shown to reduce blade root flap-wise fatigue up to 10% and ultimate loads up to 8% by Bagherpour [18]. This research demonstrated the connection between load alleviation and the ply offset angle of the materials. Further investigation has been executed by Manolas [19] on the combined use of BTC, IPC and individual flap control (IFC) which resulted in many load allaying solutions. An important conclusion which was drawn, is the increase on the pitching damage equivalent load and significant increase of ultimate loads. Combinations of AT solutions were investigated in 2019 by Bortolloti [20] who implemented the combinations in an automated design optimizer. The final design resulted in savings in terms of CoE due to an enlarged rotor diameter in comparison to the baseline turbine.

2.2.2. Sectional passive flaps

Another passive solution consists of leading and trailing edge flaps that react to pressure distribution over the blade or blade vibrations. As before mentioned, these solutions do not need measurements of the inflow conditions.

Free-tips

In aircraft, a gust alleviating passive flap was first proposed by Doney [21] dating back to 1940. Later in 1982, freely moving tips were proposed on helicopter blades by Stroub [22]. This method smoothed the load distribution over the blade and was later used on wind turbines as well as by van Kuik [23]. Despite significant effects on fatigue loads the project was not continued, because it was not easily scaled to other size wind turbines. However, Bottasso successfully proceeded the research on the 5MW wind turbine in 2016 [24] resulting in the concept in fig. 2.1.

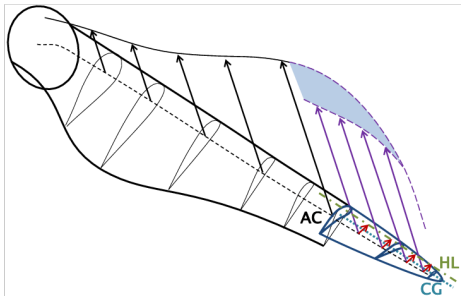

Figure 2.1: The freely moving tip concept, image courtesy of Bottasso [24].

Self-adaptive camber

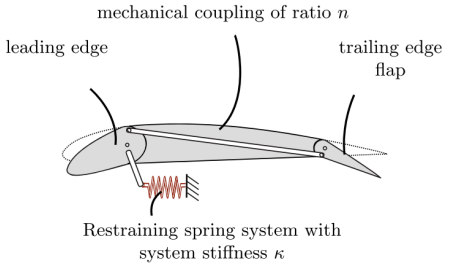

Figure 2.2: Graphical representation of the adaptive camber concept, image courtesy of [25].

A self-adaptive camber was proposed by Lambie [25–27], which combined a leading- and a trailing-edge flap showing great load alleviating potential like in fig. 2.2. The leading edge flap which experiences the greatest pressure difference, would force the trailing edge flap into a given position changing the camber of the airfoil. The mechanism connecting the leading- to the trailing-edge is, however, unrealistic to achieve without drastic changes to the internal structure of the blade.

Adaptive trailing-edge flap

Another fully passive solution is the adaptive trailing-edge flap, which was investigated experimentally in 2015, by Bernhammer [28], for aircraft. The solution reduces drag and has a piezo-electric element which can harvest from the flap deformations to perform actuation. In 2016, Navalkar et al. [29] successfully developed a numerical and analytical model for the trailing edge flap which can reduce fatigue loads on wind turbines. The flutter points were later verified experimentally by Bernhammer et al. [30].

Inertial-drive trailing edge flap

Recent research conducted in Milan proposed an inertial-driven passive flap which connects an offset mass before the trailing edge flap [31–34]. This mass is then free to move inside the free space in the blade as a reaction to blade vibrations. The mass is connected to the flap, causing the flap to move when the blade experiences an acceleration. Investigation by Bottasso [33] of the concept showed that the flap acts as a band-stop filter in the 1P-3P band, due to the synergy between the plunge and flap due to their similar frequencies. Besides that, the torsional motion remains largely unaffected in contrary to other flap configurations. Recently, in 2018 , Montinari et al. conducted a full aeroelastic multi-body analysis of the inertial-driven flap [35]. In the research it was found that the presence of the offset mass would increase the fluctuation of the edgewise bending moments. Next, the pre-load of the system was varied with rotor speed. This obliterated AEP losses but resulted in increased loads. To be more exact, *"gravity cyclically pulls on the flap, creating a radial displacement that, through the screw joint, induces a flap rotation, which in turn creates a 1P airload component that causes an increment of Damage Equivalent Load"*, says Montinari on page 174 of his recent work [35]. To augment this promising system with an active variation of the pre-load of the spring is, however, novel and will be the topic of this research.

2.3. Review of the inertial driven passive flap technology

Now the state of the art has been made clear, a review can be done on load alleviating techniques. The recent benefits that were demonstrated by the work of P. Montinari et al. in 2018 [35], are most relevant to the subject of this research. The proposed device has been depicted below in fig. 2.3 and integrates the reliability of a passive device with distributed control in the 1P-3P region. This finding is crucial, as fatigue loads are primarily present in this frequency band. Now regarding the free body diagram at the lower left in fig. 2.3. Applying a force F in the vertical direction will result in a reaction force at the hinge, given by H. Using D'Alembert's principle, this means that the offset mass m_{om} will be accelerated by a_{om} in the opposite direction. The result is the flap rotating towards the direction of the blade acceleration, resulting in a reduced amount of lift by changing the camber of the airfoil. To build upon the work that has been done by P. Montinari, the model will be augmented with an actively changing pre-load at the hinge H of the system. In practice, this can be achieved by means of a simple servo motor. The behavior is entirely compatible with the current standard wind turbine designs, i.e.: blade pitching should not excite the mechanism whereas it should change due to blade deflections. Secondly, the device should be implemented without drastic changes to the internal structure of the rotor, by sizing the offset mass and offset distance appropriately.

2.3.1. Equations of motion

The equations of motion of the flap, can be seen below in eq. (2.1).

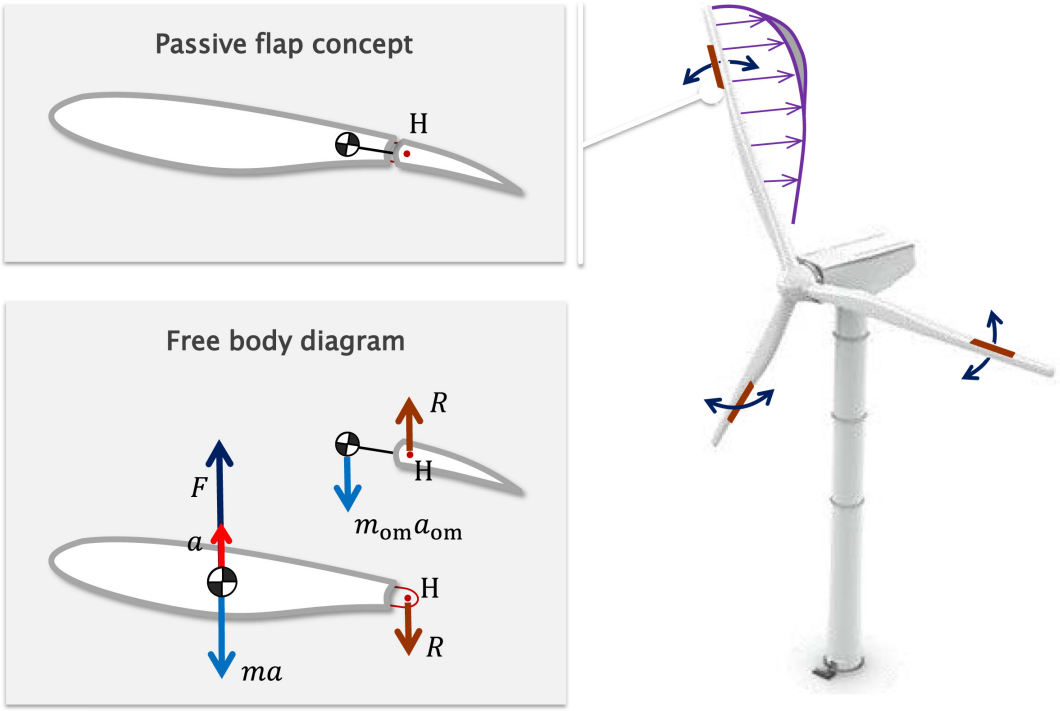

Figure 2.3: Typical section of the part of the airfoil with inertial-driven flap. Image courtesy of Montinari et al. [35].

With, flap angle δ, flap inertia J_f, spring stiffness K_f.

The right hand side consists of the aerodynamic moment M_a, the inertial moment M_i, due to blade accelerations and the pre-load M_p. The latter parameter M_p, that will be changed actively in the proposed semi-passive device. An in-depth analysis of the equations of motion and how they are implemented is discussed in chapter 3.

$$J_f\ddot{\delta} + K_f\delta = M_a + M_p + M_i \tag{2.1}$$

2.3.2. Flap parameters & performance optimization

To further optimize the performance with respect to the passive design, the flap must be tuned correctly. By tuning the pre-load, a zero mean flap deflection can be achieved to ensure the turbine is operating optimally below rated. At higher wind speeds, the flap should be more active in order to alleviate the loads effectively. Montinari et al. have recently optimized the flap parameters by calculating Weibull-weighted DELs for different configurations of the flap [35]. This has been done for blade root moments as well as tower top and base moments. The span of the flap has also been varied, increasing load authority at the cost of AEP. A summary of the findings is found below in table 2.1 and will be an excellent starting point for the implementation of the present study.

Table 2.1: Optimized parameters of the inertial-driven flap, courtesy of Montinari et al. [35].

Parameter	Value
Flap span	r/R = [0.7 0.8]
Flap chord	25% blade chord
Flap overhang	35% flap chord
Offset mass	18% sectional mass, 0.75% of total blade mass
Offset distance	21% blade chord
Flap frequency	0.014Hz (9% of 1P)
Hinge preload	Tuned for null flap deflection at 9.5m/s

2.3.3. Load reductions

The device clearly demonstrates fatigue load reductions in the flap-wise direction and many reductions in the tower. The actuator duty cycle of the pitching of the blades was found to be reduced with respect to the baseline turbine, especially at rated wind speed. The problem that fully passive solutions might be limited in use, was addressed by Bottasso in 2016 [24], who proposed a screw-joint. This solution varies the stiffness of the spring in the joint with varying rotor speed, resulting in a lower mean flap deflection, but caused an increase in DELs, due to the transmission ratio of the screw-joint. AEP loss was present up to 0.5% and 0.55% for the regular and extended span respectively, which should be reduced in further iterations. The effect on DELs have been summarized briefly in table 2.2. The edgewise blade root moments are increased which are related to the increased mass of the blade as the edge-wise moments are due to gravity. Actively changing the pre-load by means of a servo can result in better load reductions and less AEP loss. This solution results in a new, third, type of load alleviation: semi-passive flaps. Investigating the feasibility of such a design is the goal of this research.

Table 2.2: The effect of the normal and extended passive flap on DELs in % with respect to the baseline.

	Passive flap	**Passive flap, Extended span**
Main bearing	-4%	-6%
Tower Base	-7.5%	-11%
Edge	2.5%	2.5%
Flap	-7%	-9%
Torsion	10%	14%

2.4. Research Questions

The goal of this research is to demonstrate the feasibility of an inertial-driven semi-passive flap, which changes the aerodynamic behavior of the blade by reacting to blade vibrations. The pre-load of the passive flap will be controlled by an active element reducing ultimate and fatigue loads while minimizing AEP loss.

The research questions can be posed as follows:

- How does the preload change with wind speed?
  - What are key values influencing the blade section and are input to the model?
  - How do these values vary from cut-in to cut-out wind speeds?
  - What are constraints for the flap parameters?
- How well does the modeled flap compare to the DTU 10MW RWT, while simulating DLC1.2?
  - How do the fatigue loads compare?
  - How does the AEP compare?
  - How do ultimate loads compare?
- How does the semi-passive flap weigh up against other solutions?

3

Methodology

THE methodology that is used in this report is presented in depth in this chapter. This will describe the flap mechanics and aerodynamics, along with an explanation of the parameters of the flap that will be varied and their boundaries. Next, the aeroelastic code HAWC2 will be introduced, to understand the working principle behind the program and which load cases will be simulated.

3.1. Semi-passive flap mechanism

This section elaborates on the working principle of the 1 degree of freedom (DOF) system, that is the trailing-edge flap of the airfoil. The trailing-edge flap mechanism itself is shown in fig. 3.1 with the red dot depicting the hinge, to which it is connected to the remainder of the airfoil. The aeroelastic code HAWC2 uses a right handed coordinate system, with x-axis from trailing- to leading-edge and the y-axis from pressure to suction side. The z-axis then goes in to the paper, resulting in a clockwise positive flap angle denoted by δ. In fig. 3.1 one is looking down on the blade section from the hub. The mechanism relies on the acceleration of the offset mass m_{om} dominating the deflection of the flap. The movement of the mass occurs due to the blade deflecting in the x- and y-direction. The x-direction is the edge-wise direction, which is dominated cyclically by gravity. The y-direction is named the flap-wise direction affected most by turbulence. Both vibrations occur in the 1P-3P range, with P being the principal or rotation frequency. A phase shift is present as the edge-wise vibration lags behind the flap-wise movement. The flap chord is named c_f and the span, which is not visible in fig. 3.1, is named S_f. The overhang is not considered in this study, because later use of X-foil does not support changing this value. The last parameter is the spring stiffness of the hinge K_f.

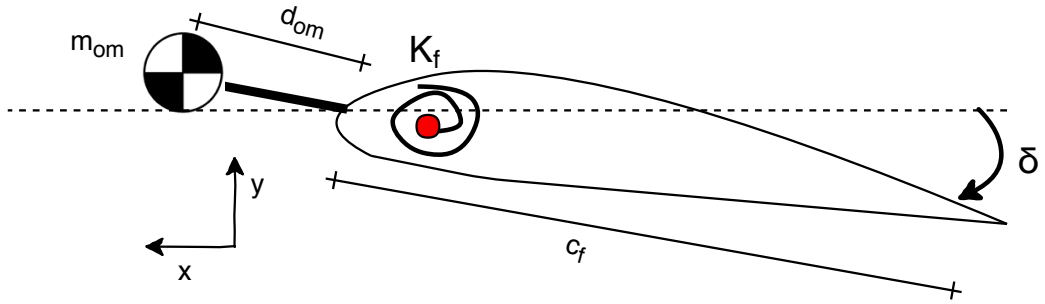

Figure 3.1: Sketch of the 1DOF system of the trailing edge flap, including the denotation of flap parameters.

3.1.1. Boundaries of the flap parameters

To remain realistic and reduce the total amount of parameter combinations, boundaries must be set to the parameters. To start, the flap chord realistically should be around 10% of the blade chord, often used in the more explored active flaps [36]. A shorter flap is chosen to not interfere with the blade internal structure, however, the recent work of Montinari [35] and Bottasso [33] show good results with larger flaps. A 20% chord flap is included in early stages of this work for completeness. The offset mass m_{om} has the negative effect

of adding mass to the blade which increases in plane loads. For this reason, the maximum added mass is capped at 30% of the blade sectional mass in early parts of the research as this greatly depends on the span. The distance of the offset mass was said to interfere with blade internal webbing of the DTU10 MW at 25% blade chord [35]. Also, the mass must have a certain distance to the hinge which was chosen to start at 5% of the blade chord. In this study, the flap span S_f is varied between a 10% and 15% of the total blade span R, specifically between [0.7 0.8]·R and [0.7 0.85]·R. Also, the minimum and maximum flap angle δ must be determined. To get a good estimate, a visual inspection was done in X-foil. First, the 20% flap was created in X-foil and deflected to -20° and to 10°, the green and the red line respectively in fig. 3.2. The green and red lines were drawn straight from the trailing edge, through the hinge.

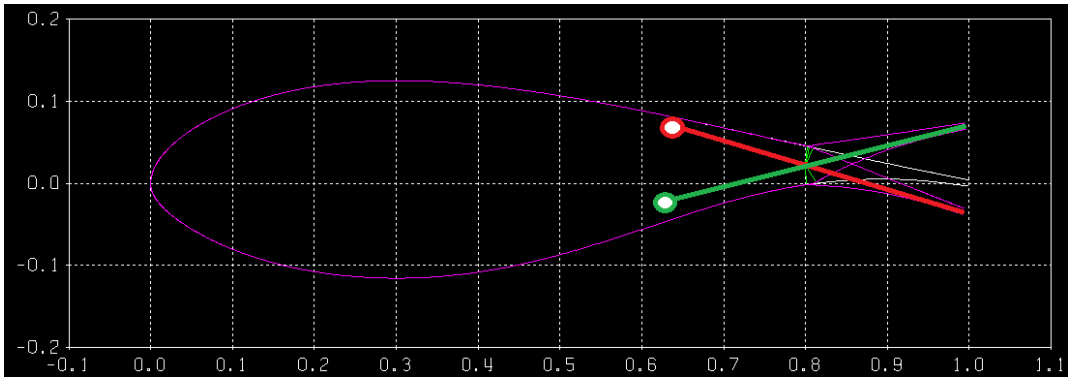

Figure 3.2: The maximum flap angles that can be seen in X-foil for the FFAW3-241 airfoil with a 20% flap at the trailing edge.

Similarly, this was done for a 10% flap which allowed a lower range of flap angles ranging from -10° to 10°. This provides a rough estimate for the flap angles.
To summarize, the range of values are shown in table 3.1. The spring stiffness range K_f is determined in chapter 4.

Table 3.1: The parameters and their respective boundaries that will be researched in the parameter study in chapter 4.

Parameter	Range
δ	[-10 10; -20 10] degrees
c_f	10%-20% blade chord
S_f	[0.7 0.8]·R [0.7 0.85]·R
m_{om}	5%-30% sectional mass
d_{om}	5%-25% blade chord

3.1.2. Dynamics of the flap

This subsection analyzes the flap behavior in response to external effects. The system has 1 DOF which is the flap deflection δ allowing to derive the equation of motion around the hinge. In this study, friction is neglected, because it scales with velocity this leaves the left hand side depending on the flap rate $\ddot{\delta}$ and the flap angle δ. The left hand side is equated to the external moments acting on the flap, resulting in the equations of motion stated below in eq. (3.1).

$$J_f\ddot{\delta} + K_f\delta = M_a + M_i + M_p \tag{3.1}$$

Starting with the left hand side, the flap rate is multiplied with the inertia of the flap, which is assumed to be dominated by the offset mass following eq. (3.2). The mass of the flap and connecting shaft is neglected. The flap angle is multiplied with the stiffness K_f of the rotational spring located at the hinge. The rotation is considered in degrees, making the spring stiffness have the unit of Nmdeg^{-1}.

$$J_f = d_{om}^2 m_{om} \tag{3.2}$$

The right hand side of eq. (3.1) consists of the external forces *id est* the aerodynamic moment M_a, the inertial moment M_i and the pre-tension of the spring around the hinge M_p.

The aerodynamic moment M_a is defined in eq. (3.3), being caused by the pressure difference over the trailing edge flap. In this equation the flap surface is the flap span S_f, multiplied by the flap chord c_f. Because a moment is considered, the flap chord is squared to multiply the force by the moment arm. The hinge coefficient, C_H, can be obtained for each specific airfoil, by use of X-foil and depends on the angle of attack, flap angle, overhang and chord. However, changing the overhang is not a possibility in X-foil, so it is considered to be out of the scope of this research. Lastly, the dynamic pressure is given by q.

$$M_a = -qS_f c_f^2 C_H \tag{3.3}$$

The next component is the inertial moment M_i which is caused by the blade vibrations and governed by the x- and y-acceleration of the offset mass a_{om}. The acceleration in the z-direction is ignored, because it only influences the dynamics by causing friction at the hinge, which is not considered. It is assumed that the movement of m_{om} does not significantly affect the blade vibrations. Following D'Alembert's principle the inertial forces acting on m_{om} are equal in magnitude but opposite in sign with the force at the hinge due to blade vibrations. Keeping in mind that the mass of the entire mechanism is assumed to be dominated by the offset mass. Here the arrow above the symbol denotes a vector. The accelerations at the hinge of the trailing edge flap can be gathered from HAWC2 data.

$$\vec{a_H} m_{om} = -\vec{a_{om}} m_{om} \tag{3.4}$$

The inertial moment around the hinge can be calculated by taking the cross product of the position of the mass with respect to the hinge, r_{om}, and the acceleration of the mass, stated in eq. (3.5).

$$M_i = \vec{r_{om}} \times m_{om}\vec{a_{om}} = d_{om}\begin{bmatrix} cos(\delta) \\ sin(\delta) \end{bmatrix} \times m_{om}\begin{bmatrix} a_{om,x} \\ a_{om,y} \end{bmatrix} = d_{om} m_{om}\Big(cos(\delta)a_{om,y} - sin(\delta)a_{om,x}\Big) \tag{3.5}$$

Lastly, the pre-load of the spring, M_p, is changed actively and is scheduled with wind speed. The mechanism behind this changing pre-load could be a small servo motor rotating the torsion spring to increase or decrease the pre-tension at the hinge. Physically this adjusts the mean of the flap deflection oscillation.

3.1.3. Obtaining hinge coefficients and sensitivity analysis

As mentioned above, the hinge coefficients were obtained from X-foil for the FFAW3-241 airfoil, which is present on the DTU 10MW blade from r = 57.8m to the tip. Obtaining these hinge coefficients from X-foil is time consuming, so, varying parameters that influence these coefficients is minimized. Primarily, the different flap chord and the Reynolds number are considered in this part. The range of flap angles were determined prior via X-foil and the range of angles of attack is taken from statistics of the DTU10 MW reference turbine, which can be seen in fig. 4.2. Because the flow is viscous one Reynolds number for below and one for above rated is calculated. The Reynolds number was determined for the average blade chord c of 3.25m, a relative velocity V_{rel} taken at mid flap (r = 0.75·R) and a kinematic viscosity of $\nu = 1.47e^{-5}\text{m}^2s^{-1}$ via eq. (3.6).

$$Re = \frac{V_{rel}c}{\nu} \tag{3.6}$$

The average relative velocity can be read from fig. 4.4 for the baseline simulation, being 45ms^{-1} and 70ms^{-1} for below and above rated, respectively. This results in the corresponding Reynolds numbers of 10e6 and 15e6, respectively. The polars for the FFAW3-241 in HAWC2, however, were obtained for a Reynolds number of 12e6. For this reason a sensitivity analysis was done on the change of the hinge coefficients with Reynolds. The difference in % of the hinge coefficient can be seen below in table 3.2 for Re = 12e6 and 15e6.

Table 3.2: Sensitivity of the hinge coefficients with Reynolds for different combinations of flap angles and angle of attack. The percentage is how much the hinge coefficient has changed at Re = 15e6 compared to Re = 12e6 for angle of α and δ.

$\alpha \setminus \delta$ [deg]	**-10**	**0**	**10**
-5	-1.6%	2.9%	0.9%
0	0%	2.4%	0.9%
15	2.7%	0.8%	0.9%

From the table it is evident that the hinge coefficients only change slightly with Reynolds. So, to stay consistent with the HAWC2 polars Re = 12e6 is used for the above rated hinge coefficients.

3.1.4. Implementation challenges

There are several challenges and downsides to the implementation of the mechanism which will be discussed in this subsection. Compared to active solutions the semi-passive solution is more robust because it relies less on real time measurements and actuation. This will affect the amount of added components and maintenance necessary for the mechanism. However, compared to having no flap, the system decreases robustness and calls for more maintenance, decreasing overall reliability. Also, implementing the system in a blade is challenging for large flap spans as the blade twist causes the flap axis to have an offset. Moreover, the offset mass must be able to move freely within the blade structure; increasing the span increases the complexity of the system because the internal structure does not change linearly. Another complication is that the offset mass might knock against the inside of the blade, which results in noise, accumulation of damages or other unwanted dynamic effects. Quite trivial is that adding the offset mass increases the blade sectional mass, negatively affecting edge-wise loading on the blade due to gravity. Torsion loads on the blade section also increase due to the pitching moment generated by the flap.

3.2. FFAW3-241 airfoil

The airfoil present at all span-wise distributions of the flap is the FFAW3-241. The polars for this airfoil have been obtained through Computational Fluid Dynamics (CFD) for a 10% chord flap, no overhang and for Reynolds of 12e6. The polar has been generated for all angles of attack and flap deflections of ±50 degrees and includes the steady lift, attached lift, fully separated, drag and moment coefficients. The attached and fully separated coefficients are used with the ATEFlap model used in HAWC2, which is explained in section 5.1.4. This airfoil is present on the blade spanning from $r = 0.6 \cdot R$ to the blade tip.

3.3. HAWC2

For clarity, a short introduction to HAWC2 is given, but more in-depth information can be found in the latest version of the manual [37]. The aeroelastic code HAWC2 has been developed with the intent to simulate the response of a wind turbine in the time domain. The code has been developed by the National laboratory of Denmark in Risø.

The code relies on the structural part of the turbine, interacting with aerodynamic properties of the entirety. The structural part relies on the use of a multi-body formulation, which assembles the structure out of smaller bodies. Each body is a Timoshenko beam element which takes into account shear deformation and rotational bending effects. This makes it suitable for sandwich composite structures and thick beams. Using this formulation large rotations and complex structures can be handled. The resulting turbine is an assembly of bodies connected by constraints which can, for instance, fix any translation and rotation at a node or allow a rotation around one axis to e.g. simulate a bearing.

The next part considers the aerodynamics, which is based on blade element momentum theory. Each blade section is defined along the `c2_def` line which defines the pre-bend and pitch angle of the half chord line of each airfoil section. The airfoils are defined by their span-wise position, chord and thickness to chord ratio. The most slender airfoils at the tip and the round cylindrical airfoils at the root. The classical blade element method is extended to handle dynamic inflow, yaw, skew angles as well as large deflections. A dynamic stall model is also present, making use of the indicial response exponential function including steady and dynamic effects due to trailing edge flap deflections; a more in-depth description is written by L. Bergami and M. Gaunaa [38]. Turbulence models as Mann- and flex-turbulence can be chosen. The applied settings are discussed in chapter 5.

All the above settings are combined in the `.htc` file, which connects them. This file is placed in a certain file structure where it finds data files, the dlls, log files and the generated turbulence. Using the same turbulence seeds for different designs allows for better comparison. Finally, the files are saved in the results folder, ready for the post processing app Pdap, or for analysis in MATLAB.

3.3.1. DTU 10 MW reference turbine

The DTU10 MW reference turbine [9] is considered throughout this report and is named the Reference Wind Turbine (RWT) or baseline model. This model is used as comparison to the turbine augmented with flap. The general parameters of the three-bladed upwind turbine are stated below in table 3.3.

Table 3.3: Main parameters of the DTU10MW reference turbine [9].

Parameter	Value
Rotor Diameter	178.3 m
Hub Height	119.0 m
Wind Class	IEC 1A
Rated-Power	10MW
Cut-in wind speed	4 ms^{-1}
Cut-out wind speed	25 ms^{-1}
Rated wind speed	11.4 ms^{-1}
Max tip speed	90.0 ms^{-1}

3.3.2. Design Load Cases (DLC)

The turbine will be assessed using the design load basis, which is DTU's interpretation of the IEC61400-1ed3 standard for onshore turbines [39]. As the mechanism is designed to reduce fatigue loads in normal turbulence, dlc1.2 is simulated. DTU describes dlc1.2 as *'simulations of power production without faults performed for wind speeds in the entire operational range with normal turbulence according to the IEC class. Yaw errors during normal operation are set to +/- 10 deg. Six seeds per wind speed and yaw error are used'* [39]. This is summarized below in table 3.4.

Table 3.4: Summary of dlc1.2 as described in [39].

Parameter	Value
Length	600 s
Wind	4 - 26 ms^{-1} in steps of 2 ms^{-1}
Yaw	-10/0/+10 deg
Turbulence	NTM, 6 seeds per wind speed and yaw error
Shear	Vertical and exponent of 0.2
Gust	None
Fault	None

Post processing the data that is acquired by sensors on the wind turbine is done by rainflow counting. First, this is done for all yaw-directions and turbulence-seed per wind speed. This results in three hours of normal operation per wind speed. The load spectra of the separate wind speeds are then combined into a life time load spectrum. Finally, using the Palmgren-Miner rule of damage accumulation, the total damage can be calculated and extrapolated to the turbine's lifetime.

4

Analytical Model

THE first simulations consist of a mathematical model of the equations of motion. The goal of this simulation is to find good combinations of parameters by running fast, low fidelity simulations in MATLAB and testing the flap model. Because full dlc1.2 simulations in HAWC2 can easily take up to 20 hours per set of parameters, this study reduces computation time dramatically. Where HAWC2 is able to get input from inflow conditions at each time-step, this analytical model relies on statistics, gathered from the baseline simulations of the DTU 10MW turbine. Gathering these statistics by placing sensors on the baseline model, is the first step of this analysis. Finally, combinations of all parameters are simulated and sorted according to certain criteria with the goal to find promising combinations to implement into HAWC2.

4.1. Statistics of the DTU 10MW reference turbine

To obtain realistic input for the mathematical model the DTU 10MW reference turbine is analyzed in HAWC2. The standard IA turbine is analyzed while simulating dlc1.2 for ultimate loads and fatigue from cut-in to cut-out. During this simulation data can be acquired by adding sensors on the aeroelastic model, which can record values as position, orientation, velocity and acceleration at a certain point. Forces and moment vectors can also be obtained using sensors. Using the post-processing app called Pdap, which is designed for use with HAWC2, plots can be made of statistics, mean, min and max values gathered from the sensors. Also, the time varying signal of each sensor can be viewed separately for each case.

4.1.1. Choosing and placing sensors

At this point it is important to define which sensors are necessary and where they are placed. Gathering information on wind speed and rotational velocity of the rotor are standard outputs of the code. Extra sensors must be placed to gather measurements on data at specific positions:

- Angle of attack α
- Relative velocity V_{rel}
- Rotational speed rpm
- Blade accelerations
- Sectional orientation of the blade

Angle of attack

The angle of attack is one of the most crucial outputs from the simulations, because it varies with wind speed, rotational speed of the rotor and defines working conditions for the airfoil and the flap. The sensor is placed at the center of the flap, which spans from $0.7 \cdot R$ to $0.8 \cdot R$ with R the total length of the rotor blade excluding the hub, this results in a radial position of $r = 64.76$m. The angle of attack is then defined in the blade sectional reference frame, its orientation with respect to the blade root, or master body, can be seen in fig. 4.1. The blade section center line, or `c2_def` line, is the position of the half chord line including pre-bend and twist with

respect to the blade root. The blade root coordinate system uses subscript *mb* and the `c2_def` coordinate system uses subscript *c2*.

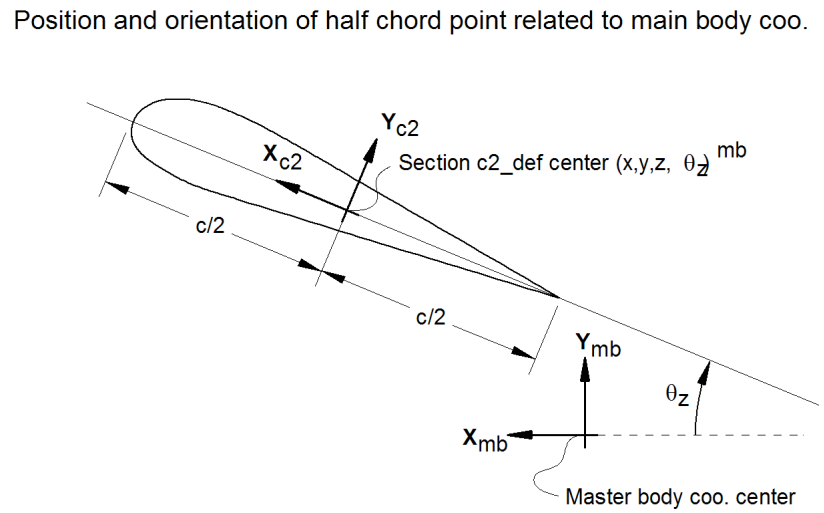

Figure 4.1: The orientation of the blade sectional coordinate system with subscript c2, with respect to the master body coordinate system centered at the blade root, with subscript mb. Image taken from HAWC2 documentation **??**.

The output of the sensor in HAWC2 is shown in fig. 4.2 which consists of the mean value in blue and the minimum and maximum value. As input for the MATLAB model the mean value for α is used as a constant for each wind speed.

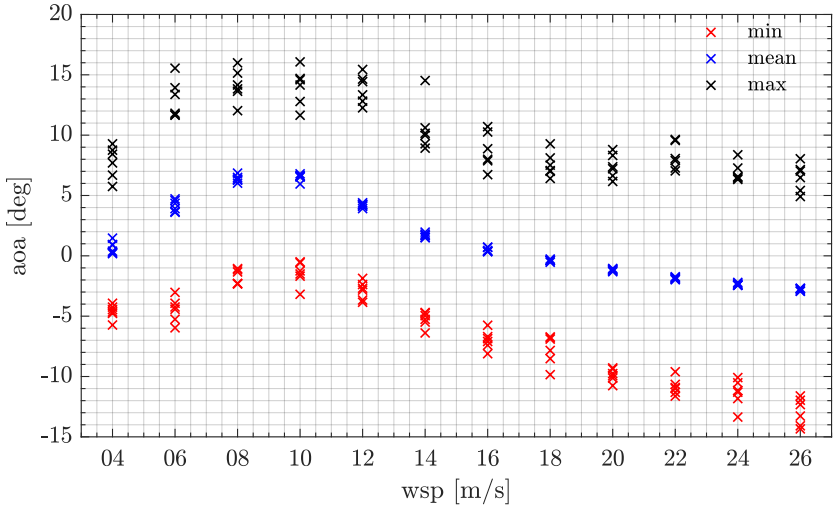

Figure 4.2: Mean, minimum and maximum values of the angle of attack from cut in to cut out wind speeds experienced by the blade section.

Blade rotational speed

The average rotational speed of the turbine at different wind speed is important for calculations in the Matlab file. Also, for calculating the 1P excitation frequency these values have importance. The principal frequency is, later, used for creating the oscillating blade acclerations. The results from the HAWC2 baseline simulations are presented below in fig. 4.3.

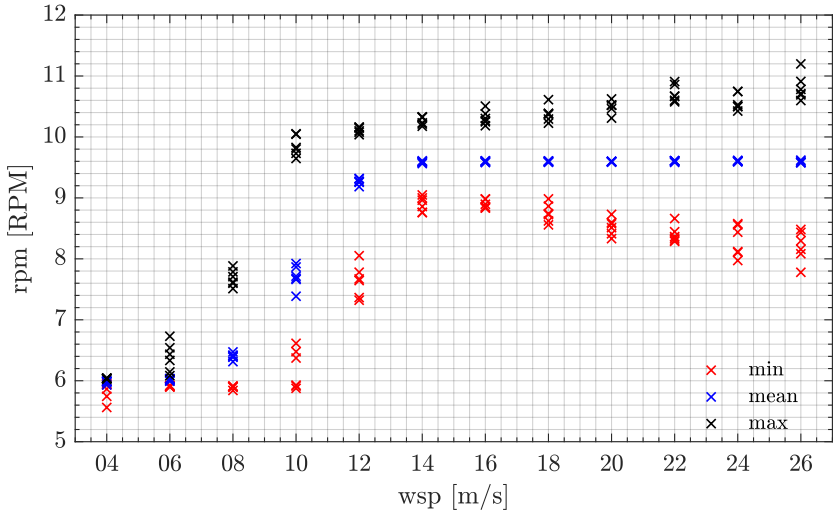

Figure 4.3: Mean, minimum and maximum values of the rotational speed of the turbine from cut-in to cut-out wind speeds.

Relative velocity

The angle of attack is closely related to the relative velocity experienced by the airfoil. The sensor for this parameter is set at the same point as the angle of attack; at the center of the flap at r =64.76m from the blade root. The orientation of the velocity is in the blade sectional reference frame. Similar to the angle of attack, the mean value of the relative velocity is used as a constant value per wind speed in these simulations.

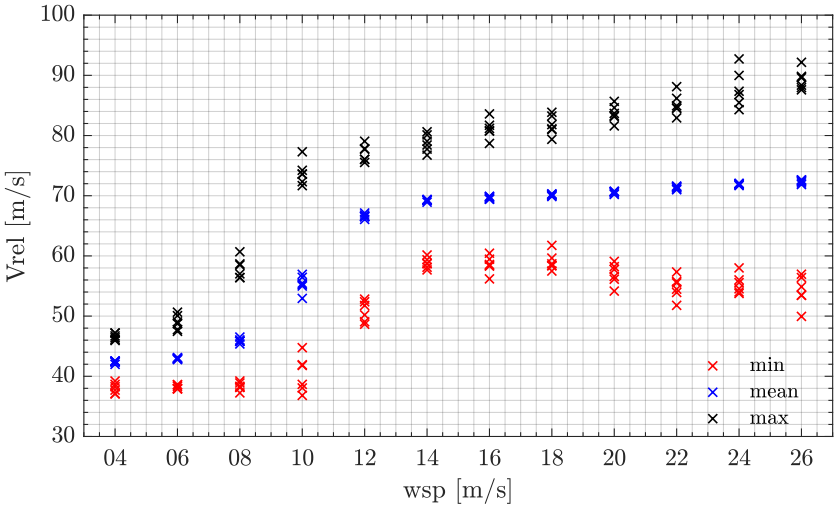

Figure 4.4: Mean, minimum and maximum values of the relative velocity seen by the airfoil from cut-in to cut-out wind speeds.

Blade accelerations

The blade accelerations are necessary as the concept used in this research acts due to blade vibrations. The accelerations in the span-wise direction are ignored due to the assumption that there is no friction present. Obtaining these values is done at the mid flap position, but can only be obtained in the blade root coordinate system. All accelerations will have to be rotated to the blade section coordinate system. Because these vibrations are dominated by the 1P frequency they will later be made into time varying signals. The variation of the x-acceleration around a zero mean for a_{mb} is visible in fig. 4.5. For the y-accelerations a slight offset is present above rated wind speeds, this bias is taken into account in the input.

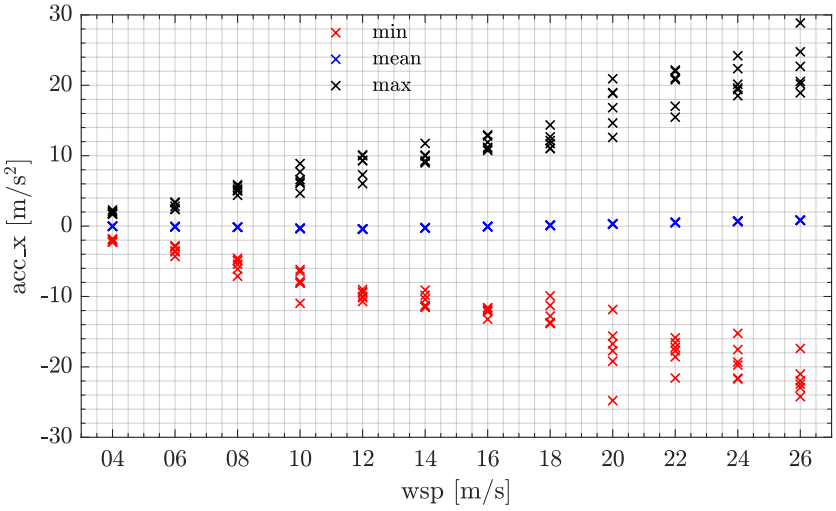

Figure 4.5: Accelerations in the x_{mb} direction for each wind speed. The mean of the accelerations is approximately zero.

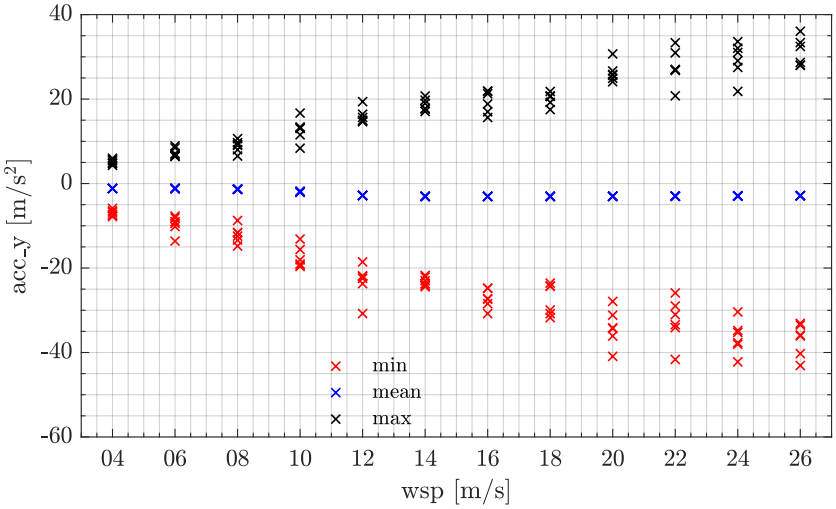

Figure 4.6: Accelerations in the y_{mb} direction for each wind speed. The mean of the accelerations is in this case non zero, which should be taken into account.

Sectional orientation

The sectional orientation of the blade section is needed in combination with blade accelerations, as they can only be obtained in the blade root coordinate system. In this case a sensor is added at the blade section center which gives the rotation of the $c2$ coordinate system with respect to the blade root mb coordinate system. The output is a set of three *Euler angles* yielding the rotation about the x, y and z angle respectively. For brevity all the mean values of the blade accelerations have been plotted in fig. 4.7. The rotation around the x_{mb}-axis starts positive and follows the line one expects from the thrust curve: peaking at the rated wind speed, where the blade creates most lift. The rotation around the y_{mb}-axis represents an edge-wise rotation. This rotation is rather constant over the operating range, but causes a rotation in the opposite direction of the rotation. This curve also peaks at rated wind speed. Above rated the turbine starts pitching reducing the lift and the rotation of the blade. Lastly, the rotation around the z_{mb}-axis represent a rotation towards the wind which is mainly due to the pitching of the blade section.

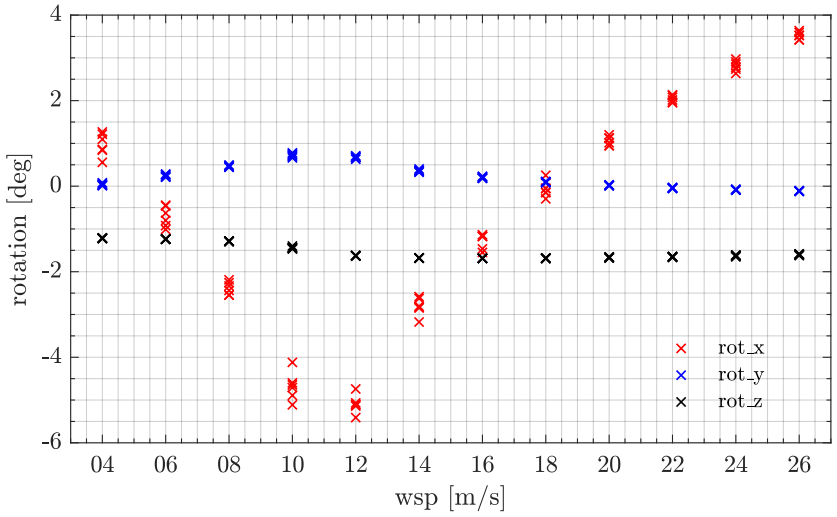

Figure 4.7: The mean value of the Euler angle signals from HAWC2.

Following the right handed coordinate system that HAWC2 uses, the following rotation matrices are used to rotate the accelerations from the main body frame to the blade section frame by eqs. (4.1) to (4.3).

$$R_x = \begin{bmatrix} 1 & 0 & 0 \\ 0 & cos(\theta_x) & -sin(\theta_x) \\ 0 & sin(\theta_x) & cos(\theta_x) \end{bmatrix} \tag{4.1}$$

$$R_y = \begin{bmatrix} cos(\theta_y) & 0 & sin(\theta_y) \\ 0 & 1 & 0 \\ -sin(\theta_y) & 0 & cos(\theta_y) \end{bmatrix} \tag{4.2}$$

$$R_z = \begin{bmatrix} cos(\theta_z) & -sin(\theta_z) & 0 \\ sin(\theta_z) & cos(\theta_z) & 0 \\ 0 & 0 & 1 \end{bmatrix} \tag{4.3}$$

Obtaining the total rotation matrix C is done by multiplying the separate rotations as below in eq. (4.4).

$$C = R_x R_y R_z \tag{4.4}$$

Then rotating the accelerations from the main body coordinate system a_{mb} to the blade section accelerations at the hinge a_H is done following eq. (4.5).

$$a_H = C a_{mb} \tag{4.5}$$

Obtaining the accelerations of the offset mass, a_{om}, is done by following the previously explained eq. (3.4). For the amplitude of the x- and y-accelerations the maximum value was taken and varied sinusoidal. The two time-dependent accelerations act out of phase as the edge-wise component is dominated by gravity and the flap-wise y-component is dominated by turbulence and the blade position. Now, the accelerations are varied periodically at each time step t with the 1P frequency f, resulting in the time varying accelerations in eq. (4.6).

$$\vec{a_{om}}(t) = \begin{bmatrix} a_{om,x} sin(2\pi f t) \\ a_{om,y} cos(2\pi f t) \end{bmatrix} \tag{4.6}$$

4.2. Assumptions and approximations

Several assumptions have already been mentioned in the previous text and are summarized below:

- Artificial periodic blade acceleration changes with 1P frequency
- No damping due to neglected friction assumption at the hinge
- Constant relative velocity per wind speed
- Constant angle of attack per wind speed
- Constant rotational speed per wind speed

- Flap mass is negligible compared to the offset mass
- Flap mechanism is rigid
- Steady aerodynamics

4.3. Implementation of model in MATLAB

To implement the equations presented in chapter 3, a script has been written in MATLAB, which has been appended in appendix A. After defining constants, all the structural data and input from the HAWC2 baseline is imported, these are stored in matrices per wind speed. Now, a combination of the parameters from table 3.1 is chosen creating a *case* which is given a number. For each of these cases the entire operating range of wind speeds is simulated. The simulations last 100s, which is enough to gather statistics in these non turbulent conditions.

4.3.1. Time integration method

To implement the equation of motion eq. (3.1) into the MATLAB file, they must first be rewritten and then a time marching scheme must be selected. The rewritten formula is stated below in eq. (4.7). All the terms on the right hands side are known at a given time n and thus $\ddot{\delta}$ can be solved for.

$$\ddot{\delta}_n = \frac{-K_f\delta + M_a + M_i + M_p}{J_f} \tag{4.7}$$

Using the calculated $\ddot{\delta}$ the new values for $\dot{\delta}$ and δ can be calculated. For the first simulations, the built in `ode45` solver was used, which adopts the Runge Kutta 4th order method. The time step Δt that is used is chosen similar to that in HAWC2, which is 0.01s. Several methods were compared among which *Forward Euler*, *Midpoint Rule*, *Runge Kutta 4th order* and a variation called *Euler-Cromer*. The last method is used in further calculations, because it gives similar results to the `ode45`, *Runge Kutta 4th order*, but being 1st order it reduces computation time. The scheme involves calculating the new flap velocity as in eq. (4.8) which is the same as regular *Forward Euler*.

$$\dot{\delta}_{n+1} = \dot{\delta}_n + \ddot{\delta}_n \Delta t \tag{4.8}$$

This step differs from *Forward Euler* as it uses the newly calculated $\dot{\delta}_{n+1}$ to calculate the new flap angle in eq. (4.9). This method has proved to be stable for oscillating systems.

$$\delta_{n+1} = \delta_n + \dot{\delta}_{n+1} \Delta t \tag{4.9}$$

Besides that this method costs less computational power it allows for the implementation of a mechanical stop which was not possible using the `ode45` solver. This mechanical stop ensures that flap angles do not exceed their maximum. Using `ode45` the flap deflection reaches nonphysical flap deflections, where the offset mass passes through the blade structure. This resulted in `NaNs` because the flap deflection exceeds the range of hinge coefficients that were obtained from X-foil.

4.3.2. Tuning method of the preload Mp and sensitivity of flap deflection

Solving the above equations, results in a flap angle as a function of time. The output is dominated by the inertial moment, which is a periodic signal. The mean of this flap angle will, in most cases, show a non-zero value. If a non-zero mean flap angle is present, this could result in the blade not performing efficiently. By tuning the pre-load, M_p, a mean flap angle within a half degree of zero is achieved by tuning. By implementing a set of `IF`-statements in the MATLAB code a new M_p is chosen on the basis of the resulting mean flap deflection.

- `IF` the flap deflection is negative and has changed less than 0.05 degrees: increase M_p by 10Nm.
- `IF` the flap deflection is positive and has changed less than 0.05 degrees: decrease M_p by 10Nm.
- `IF` $\delta > 1$, decrease M_p by 5Nm.
- `IF` $\delta < -1$, increase M_p by 5Nm.
- `IF` $0 < \delta < 1$, decrease M_p by 2Nm.

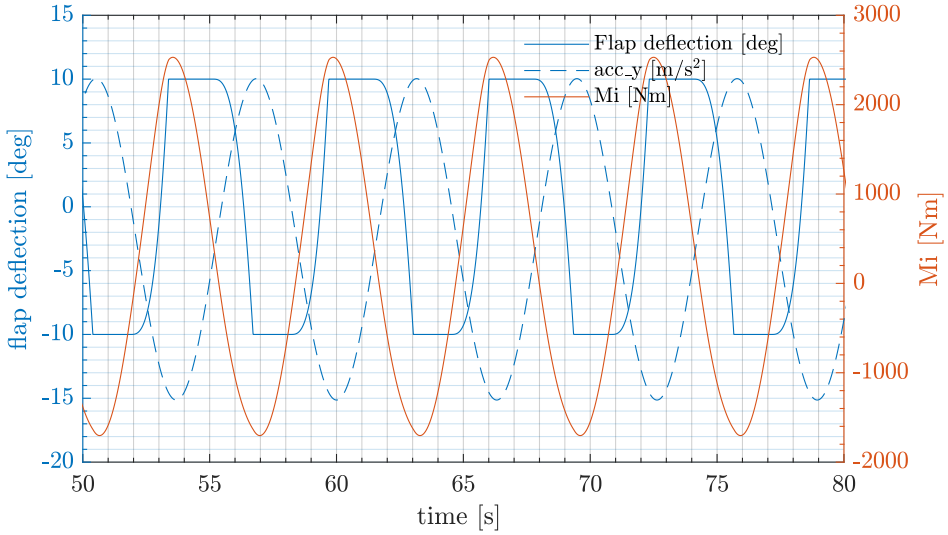

Figure 4.8: The flap deflection time response to the out-of-plane acceleration in the same figure.

- IF $-1 < \delta < 0$, increase M_p by 5Nm.

When a pre-load has been found that results in a satisfactory mean flap deflection, this pre-load is used as the starting point for the next wind speed. Once all wind speeds have been tuned, the pre-loads, mean flap deflections and standard deviations of the flap deflections are stored for each *case*. In this fashion just under 1000 cases were calculated and the parameters and results stored. With new iterations the amount of cases reduced .

4.3.3. Flap response

The output of the model is a time series of the flap angle reacting to input. To check if the flap is behaving as one would expect, the flap deflection is shown in the same figure as the out-of-plane acceleration in fig. 4.8. Here, a negative out-of-plane acceleration is when the blade is moving upwind. In this case the flap should deflect towards the free stream, which are positive flap angles. The positive flap angle increases lift at the blade section causing it to decelerate and reduce the amplitude of oscillation. Opposite, a positive out-of-plane acceleration moves the blade down wind. Here the flap moves to negative flap angles, rotating counter clockwise and reducing the lift on the blade section. Again decelerating the blade movement and reducing the oscillation. A second aspect of fig. 4.8 is the right hand side axis, which shows the inertial moment M_i. Comparing the phase of M_i to the out-of-plane acceleration, shows that when the blade accelerates upstream, the inertial moment becomes positive. This increasing moment results in the positive flap angle. The dependency of M_i on the out-of-plane acceleration is evident in this figure. A slight lag visible between the two which is due to the in plane acceleration contributing to M_i.

4.3.4. Sorting of results

To get an idea of a promising set of parameters, one can only look at the resulting flap deflection and statistics hereof. The standard deviation of the flap deflection is a measure for the flap activity. As the blade operates most efficiently below rated the flap mean should be close to zero to maximize AEP. Flap activity should be high above rated to reduce fatigue. The results were assessed for wind speed of 14ms^{-1}, in terms of how much the flap changes the lift in the blade section compared to the baseline configuration. The calculation is done by taking the standard deviation of the flap deflection and determining the lift coefficient at this α and δ. Taking the ratio of the new lift to that of the baseline, one obtains eq. (4.10) with Cl_f and Cl_b for the configuration with flap and the baseline respectively. The change in lift ΔL is given as a percentage. The results were then sorted for the load alleviating potential resulting in table 4.1.

$$\Delta L = \frac{0.5\rho S_f V_{rel}^2 Cl_f}{0.5\rho S_f V_{rel}^2 Cl_b} = \frac{Cl_f}{Cl_b} \cdot 100 - 100 \tag{4.10}$$

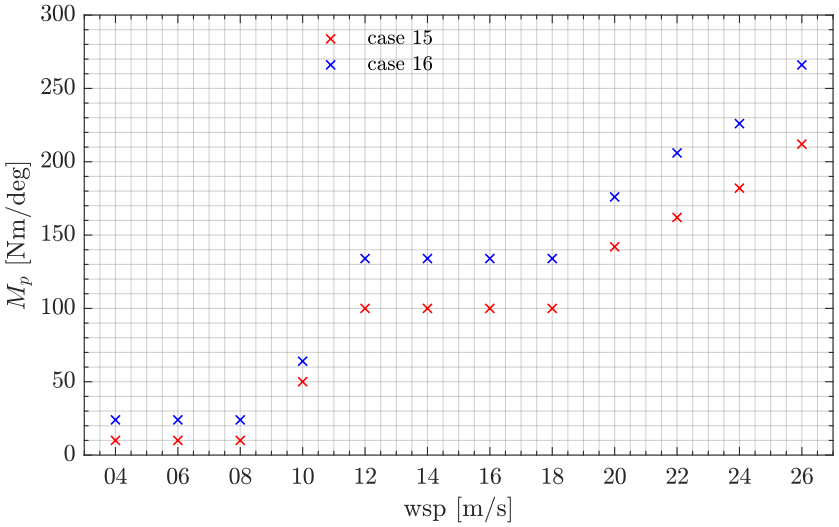

Figure 4.9: The calculated distribution of the pre-load for each wind speed of the low-fidelity model. The shown cases are 15 and 16 from table 4.1.

4.4. Results & Discussion

The result of the simulations are large table with combinations of parameters that offer high load alleviation. More findings consist of the actuator rotation limits. Lastly, the change in pre-load for each wind speed is shown in a figure.

4.4.1. Resulting table of cases

The resulting table is shown in table 4.1. Here it is visible that the spring stiffness values are generally at the lower end of the parameter range, resulting in higher flap activity. This might call for an even lower spring stiffness in further iterations. Further the larger flap chord showed higher load alleviation possibilities which is intuitive. But, it is less realistic to implement and the polar diagrams for 20% flap were not available so these results were discarded. In the table it also states if the offset mass would reach the maximum flap angle. This would result in the offset mass hitting the inside of the blade possibly causing damages and unwanted noise. It was found that most cases would hit the inside of the blade. The last column is discussed in the next two sub-sections. .

4.4.2. Change of pre-load with wind speed

This part answers the first research question, how the M_p changes with wind speed. The pre-loads are stored in `.mat`-files from MATLAB. For the cases 15 & 16 the required pre-tension has been plotted in fig. 4.9. M_p changes are dominated by the blade vibrations, which, as seen in figs. 4.5 and 4.6 are continuously increasing. This trend is also clearly visible for cases 15 and 16.

4.4.3. Actuator rotation range

Returning to table 4.1, the last column shows the total rotation the pre-load actuator must achieve, to reach the range of pre-loads. This has been calculated following equation eq. (4.11), resulting in the total rotation, ϕ.

$$\phi = \frac{M_p}{K_f} \tag{4.11}$$

The total rotation ϕ_{total} can be obtained by deducting the minimum rotation from the maximum rotation as in eq. (4.12). In the table it is visible that cases with low stiffness and high m_{om} have the largest operating range. Also the larger span generally increases the load authority and operating range.

$$\phi_{total} = max(\phi) - min(\phi) \tag{4.12}$$

Table 4.1: Table of the results of the parameter variation study. For each case the parameters ad results can be seen.

Case	K_f [Nm/deg]	m_{om}	d_{om}	chord	span[r/R]	ΔL 8ms^{-1}	ΔL 14ms^{-1}	ϕ_{total}[deg]
16	40	30%	10%	10%	15%	31.32	61.45	6.05
15	40	30%	10%	10%	10%	31.19	61.4	5.05
10	40	20%	10%	10%	15%	31.06	61.36	4.35
14	40	30%	5%	10%	15%	30.92	62.74	3.4
9	40	20%	10%	10%	10%	30.69	61.27	3.05
18	40	30%	20%	10%	15%	30.09	59.24	11.2
17	40	30%	20%	10%	10%	30.08	59.23	8.7
12	40	20%	20%	10%	15%	30.07	59.23	7.45
11	40	20%	20%	10%	10%	30.03	59.22	5.95
36	100	30%	20%	10%	15%	29.95	59.2	4.88
6	40	10%	20%	10%	15%	29.85	59.18	4.2
35	100	30%	20%	10%	10%	29.8	59.17	4.08
30	100	20%	20%	10%	15%	29.62	59.14	3.54
5	40	10%	20%	10%	10%	29.59	59.13	3.45
29	100	20%	20%	10%	10%	28.71	59.05	2.7
54	200	30%	20%	10%	15%	28.13	59.04	2.6
34	100	30%	10%	10%	15%	27.58	61.13	2.7
13	40	30%	5%	10%	10%	27.29	62.56	2.6
53	200	30%	20%	10%	10%	25	58.88	2
8	40	20%	5%	10%	15%	24.91	62.4	2.4
4	40	10%	10%	10%	15%	24.14	60.97	2.4
33	100	30%	10%	10%	10%	24.05	60.9	2.02
48	200	20%	20%	10%	15%	24.01	58.72	1.7
24	100	10%	20%	10%	15%	24	58.72	1.78
28	100	20%	10%	10%	15%	21.58	60.68	1.74
3	40	10%	10%	10%	10%	21.27	60.63	1.65
23	100	10%	20%	10%	10%	20.49	58.3	1.32
47	200	20%	20%	10%	10%	20.49	58.31	1.3
7	40	20%	5%	10%	10%	20.28	62.01	1.6
27	100	20%	10%	10%	10%	19.14	60.13	1.24
52	200	30%	10%	10%	15%	18.93	60.02	1.16
32	100	30%	5%	10%	15%	18.82	61.05	1.02
2	40	10%	5%	10%	15%	16.39	58.29	0.5
51	200	30%	10%	10%	10%	16.3	57.98	0.66
42	200	10%	20%	10%	15%	15.58	53	0.51
31	100	30%	5%	10%	10%	15.28	56.93	0.4
22	100	10%	10%	10%	15%	13.77	51.6	0.32
46	200	20%	10%	10%	15%	13.76	51.72	0.3
26	100	20%	5%	10%	15%	13.06	53.05	0.1
1	40	10%	5%	10%	10%	12.68	51.95	0.25
41	200	10%	20%	10%	10%	11.53	46.61	0.35
21	100	10%	10%	10%	10%	10.53	44.47	0
45	200	20%	10%	10%	10%	10.52	44.69	0
25	100	20%	5%	10%	10%	10.13	41.84	0
50	200	30%	5%	10%	15%	9.75	40.75	0
49	200	30%	5%	10%	10%	7.56	36.37	0
40	200	10%	10%	10%	15%	6.63	40.58	0
20	100	10%	5%	10%	15%	6.48	35.63	0
44	200	20%	5%	10%	15%	6.46	35.72	0
39	200	10%	10%	10%	10%	5.12	29.5	0

The last column of table 4.1 that either an actuator with high rotational precision is necessary or that a transmission is needed for the mechanism. Adding such complexity might decrease robustness and increase the mechanism cost.

4.4.4. Recommendations

With the current low-fidelity model there are several things that can be done to increase its fidelity. Some assumptions in the model can also be improved in later iterations, when the mechanism comes closer to a final design.

- Increase fidelity of input: the blade acceleration input could be taken from HAWC2 signals. In stead of using statistics, the time series of the signal could be fed into the model. The same could be done for the angle of attack and relative velocity.
- Add damping to the system in the form of friction a the hing bearing. This only adds a single term in the equation of motion, as the flap velocity is already calculated. Only an estimate of the hinge friction coefficient is necessary to achieve this.
- Increase resolution of flap parameters after each iteration or after simulating in HAWC2.
- Obtaining hinge moment coefficients C_H from a another program than X-foil could speed up this process. This allows for inspection of more Reynolds numbers and a new parameter: flap overhang.

4.5. Conclusions

This chapter answers the first research question and its sub-questions. The first sub-question was what the key values are that influence the blade section and are input to the model? The key parameters are:

- α
- V_{rel}
- rpm
- Blade accelerations
- Blade rotation

The next sub-question was, how these values change from cut-in to cut-out wind speeds. The answer to this question can be found in figs. 4.2 to 4.7.
The last sub-question is what the constraints are for the flap parameters which was answered in the methodology in table 3.1.
Using the answer to these sub-questions, the model was created wherein the pre-load M_p could be tuned. The result consists of multiple sets of flap parameters sorted on their load alleviating potential. From table 4.1 case 15 and 16 will be implemented first in the aeroelastic model. The research question that was answered by the sub-questions is: how does the pre-load change with wind speed? The change in pre-load was found for all the simulated cases and has the distribution of fig. 4.9.

Lastly, some final conclusions were drawn:

- Desirable flap behavior was accomplished and the flap response is as intended.
- Rotation of the driving servo motor to achieve pre-load must have high precision or a transmission is necessary, which reduces robustness of the system. The higher the load authority of the flap the higher the actuator range.
- The flap with the highest load alleviation potential uses a heavy mass close to the flap hinge. The trade-off is between creating a high mass far from the hinge increasing the inertial moment and keeping the inertia low.

5

Aeroelastic Model

BUILDING on the conclusions of the previous section the research proceeds to the aeroelastic implementation of the flap. The flap model that was used in chapter 4 is here converted into a program that can actively connect to HAWC2. This enables dynamic input to go into the flap model and the flap to have an impact the aeroelastic effects. Finally, the effect on the loads of the operating wind turbine can be compared to the baseline model without flap to estimate the reduction in loads and determine the effectiveness of the model.

5.1. HAWC2 simulation settings

There are many possible combinations of settings that can be chosen in HAWC2. For clarity the most important models concerning aerodynamics are specified. This discusses the shear format that is used, the turbulence model, the method that is used for tower shadow and the dynamic stall model for the flap.

5.1.1. Shear format

The shear format that is used is the power law which originates from Blasius' Velocity profile in 1908 [40], which accounts for the gradient in the mean wind speed following eq. (5.1). Here $\bar{u}$ is the mean of the stream-wise velocity and z is the height in the stream. The exponent a is the shear exponent which is specific for different types of stability. In all simulations a takes the value of 0.2, for slightly rough surfaces as hay or pastures [41], in normal atmospheric conditions. The values of u_0 and z_0 are the reference velocity and the reference height respectively. This method is preferred to the *log-law* due to its simplicity, making it less computationally intensive.

$$\bar{u}(z) = u_0\left(\frac{z}{z_0}\right)^a \tag{5.1}$$

5.1.2. Mann turbulence model

Turbulence is generated for each wind speed by use of the Mann turbulence model, which is built on Rapid Distortion Theory [42]. Regular isotropic turbulence has equal turbulence quantities and turbulent length scales in all three directions. This implies that turbulent structures are circular. Turbulence is, however, not isotropic, but has increased length scales and variance of the flow velocity in the stream-wise direction. This makes turbulent structures more elliptic in the stream-wise direction. Using Mann turbulence, this is accounted for by use of the Kaimal formulation of the energy spectrum which is derived in [43].

5.1.3. Tower shadow potential

Tower shadow is included, which adds a layer of complexity to the blade aerodynamics. The model that is used not only affects the flow velocity, but also takes into account the position of the tower, capturing the dynamic behavior of the position of the tower shadow.

5.1.4. ATEFlap aerodyanamic model

To model the flap the ATEFlap model is used that was developed by L. Bergami and M. Gaunaa [38]. The aerodynamic ATEFLAp model is designed to take into account steady and dynamic effects and provide output of the lift, drag and pitching moment. Input is necessary of a `.ds` file containing pre-processed data of the FFAW3-241 obtained from CFD. The dynamic effects that are added in the model are threefold:

- *Apparent mass terms*; also known as the non-circulatory part due to airfoil its movement displacing the surrounding fluid. The non-circulatory part only depends on the instantaneous motion of the airfoil and does not include memory effects.
- *Circulatory effects* due to wake shedding. These quasi-steady effects simply entail that changes in flow conditions, due to eigen-movement are accounted for.
- *Dynamic stall* captures the dynamics of the forces on an airfoil experiencing flow separation or stall.

The *dynamic stall* method is based on the Beddoes-Leishmann dynamic stall formulation [44, 45]. In this formulation the steady lift coefficient is built up out of the fully attached lift coefficient and the fully separated lift coefficient, following a weighting function. The attached lift coefficient is present when viscous effects, that occur with flow separation, are neglected. Using this premise the attached lift coefficient follows a linear relation. The weighting function varies from zero to one, with zero being fully separated and is derived from the expression of the flat plate lift in Kirchoff flow. Due to the trailing edge flap the steady lift coefficient is not only a function of the angle of attack, α, but also the flap angle, δ. Thus, all Beddoes-Leishman components rely on α and δ.

5.1.5. Concentrated mass

To account for the added mass of the mechanism, .i.e the offset mass, a concentrated point mass is added at the node situated at mid flap position. This increases the effect gravity has on the 1P edgewise moments. For flaps with larger spans, more concentrated masses are added at each node to more accurately account for the increased weight. Each concentrated mass requires the mass moment of inertia around the three axes. This simplified method was used to model negative effects the added mass has on the edgewise blade vibrations, besides the added torsion moment at the blade root. This is and added effect of this high-fidelity model.

5.2. Implementation of the .dll

The MATLAB model that was used in chapter 4 must be rewritten in the Fortran 90 programming language in order to create the `.dll` which is linked to the `.htc`-file run by HAWC2 following fig. 5.1. The code can be found in its entirety in appendix B. At the start of the time simulation the `.dll` reads in constant parameters, e.g. the flap dimensions. Then at each time step n HAWC2 calculates the new position of the turbine and flow conditions perceived by the rotor and sends relevant information to the `.dll`. Parameters are shown in the figure being the angle of attack α, time-step t_n, the old flap angle δ_n, relative velocity V_{rel}, the blade accelerations a_{mb} and blade orientation. The `.dll` then computes the new flap angle δ_{n+1} and returns it to HAWC2 for the next time-step. This process repeats until the end of the simulation time has been reached.

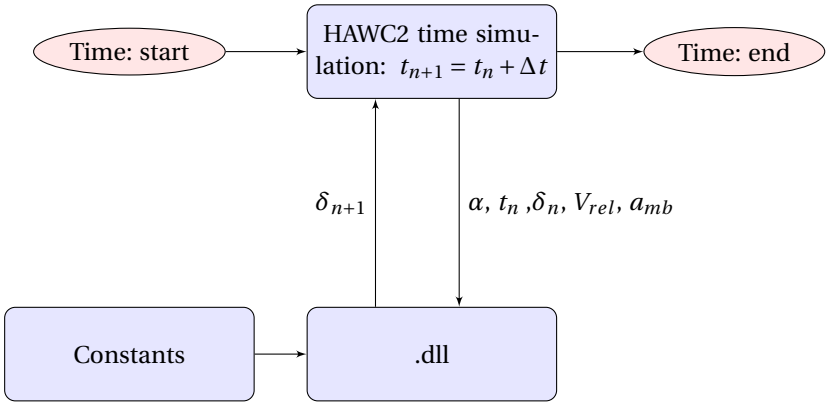

Figure 5.1: Flow chart of the time marching simulation in HAWC2 and its connection at each time step to the .dll. At the first time step the .dll imports the constant values.

As the code is in Fortran 90, the module commences by declaring all variables that are used. Then the code consists of two main parts named subroutines. The first subroutine is the *initialization* sub-routine, which only runs once during the whole time simulation. Hence, constants, like the hinge coefficients from section 3.1.3, are read into the `.dll` as seen in fig. 5.1. The second sub-routine is the *update* sub-routine, which reads the parameters from HAWC2 for all three blades at the current time-step and returns δ and $\dot{\delta}$.

5.2.1. Initialization subroutine

Besides reading the hinge moment coefficients, C_H, the initialization subroutine contains the control of the pre-load. Because the mean wind speed is the same for each separate simulation the pre-load does not vary. This simple scheduling of the pre-load reaches the same results as a more complex control implementation without over complicating the system. One could even argue that it is less computationally intensive. An example of the implementation is given below, the full scheduling is found in appendix B.

```
IF (wsp== 4)THEN ! file 1-6
mp = -17 ! Nm/deg
ELSE IF (wsp== 6) THEN ! file 7-12
mp = -8   ! Nm/deg
ELSE IF (wsp== 8) THEN ! file 13-18
mp = 0    ! Nm/deg
END IF
```

5.2.2. Update subroutine

The second part is the section that actively connects data from HAWC2 to the flap control which consists of several parts which are summarized below:

- Rotating the blade acceleration from the blade root coordinate system to the blade section coordinate system, eqs. (4.1) to (4.5).
- Calculating the inertial moment, eq. (3.5).
- Bi-linear interpolation of hinge moment coefficients to α and δ.
- Calculate aerodynamic moment, eq. (3.3).
- Solve for instantaneous flap acceleration $\ddot{\delta}$ following eq. (4.7).
- Time integration of flap acceleration $\ddot{\delta}$ and flap velocity $\dot{\delta}$ using Euler-Cromer algorithm, eq. (4.8) & eq. (4.9). This yields the new flap velocity and angle.
- Repeat former steps for remaining two blades.

5.3. Preload tuning method

The tuning method for the preload in the `.dll` must be explained, because there are significant differences between the pre-load estimated in the MATLAB model, presented in chapter 4 and the pre-load necessary in HAWC2. Discussing the source of these differences is discussed later. However, at first it was assumed that the blade accelerations oscillated around zero but there is, however, a slight offset for above rated wind speeds. This is taken into account in later iterations. As the models are similar in every way except the dynamically changing input to the model; the input must be at the source of the problem. Modeling the input more accurately could reduce the difference but an aeroelastic response would still lack. So, a tuning method was made to obtain the correct pre-load, M_p, in HAWC2 in a most efficient way. That is the topic of discussion in this section and has the structure depicted in the flowchart in fig. 5.2.

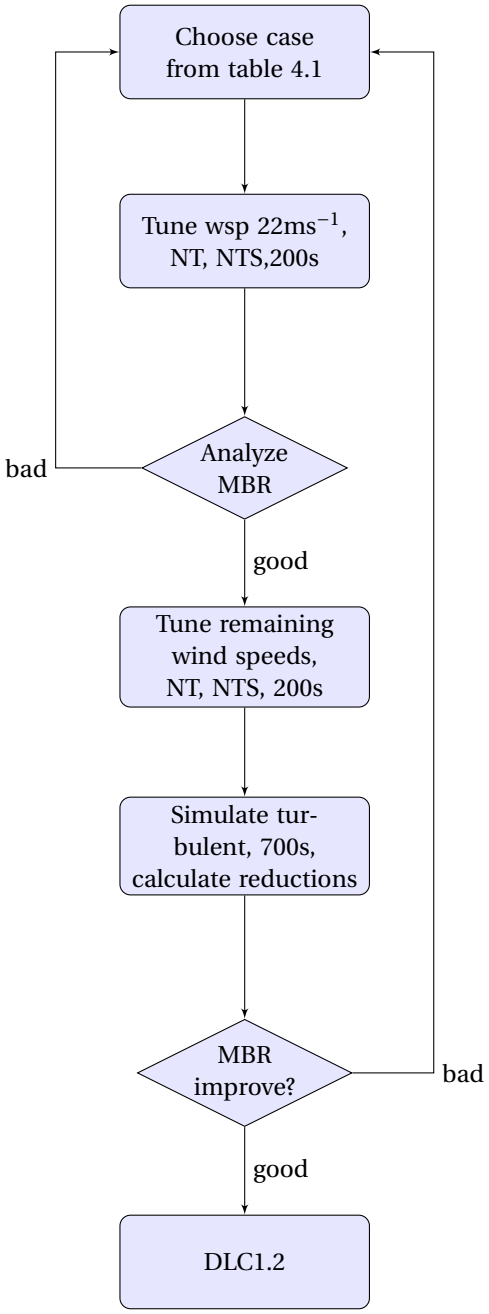

Figure 5.2: Flow chart of the tuning method to tune the preload manually in HAWC2. In this flowchart wsp refers to the wind speed. NT means no turbulence and NTS is a simulation without tower shadow. MBR are the moments at the blade root.

Choose case from table

The work flow commences with choosing a case from table 4.1, which is based on the load alleviation potential. As mentioned before, this is done by taking taking the ratio of the lift at the standard deviation of the flap deflection over that of the baseline, i.e. a flap deflection of zero degrees, as in eq. (4.10). From this table it was concluded that case 15 and 16, which have been highlighted in blue in the table, should be analyzed first. During several iterations these cases will change.

Tuning one wind speed

The process proceeds to tune the first case above rated, at wind speed 22m^{-1}. This wind speed is chosen because the oscillation of the accelerations are larger for higher wind speeds, see figs. 4.5 and 4.6. This means the flap would saturate more easily, reaching its minimum and its maximum position often at these wind

speeds. This saturation effect results in less smooth load alleviation and would cause the offset mass to hit the inside of the airfoil. Choosing this wind speed allows tuning the flap for aggressive accelerations, at a wind speed that occurs frequent compared to even higher wind speeds. The tuning is done with no turbulence (NT), no tower shadow (NTS) and for only 200s. Tuning for 200s reduces the computation time from 20 to around 5 minutes depending on the case. Using no turbulence nor tower shadow, allows to tune the pre-load most accurately for a zero mean flap angle. If turbulence were to be used, it could result in tuning the flap oscillations around a non-zero mean, negatively affecting the aerodynamics and power production. The tuning is done by changing the `If` statement in the `.dll`, which schedules a certain pre-load, as mentioned in section 5.2.1, with the mean wind speed in the `.htc`-file. Regarding the response of case 16 to a 2ms^{-1} step in wind, it was found that the response of the flap was too slow. A slow response is shown in fig. 5.3. At time=150s a wind step occurs from 20 to 22ms^{-1}. The phase of the blade root moments, shown in orange, stays similar to 1P, but the flap deflection reacts sluggish where a more immediate jump to negative values is expected. Regarding eq. (3.2), for the inertia, this parameter needs to be lower, which can be achieved by lowering either d_{om} or m_{om}. On the other hand increasing the moment due to the inertia in eq. (3.5) would results in a quicker response. This then on the contrary would mean increasing both d_{om} or m_{om}, which is contradictory to reducing the inertia. Decreasing d_{om}, however, seems most viable as this is squared in eq. (3.2). Going back to choosing a new case, resulted in choosing case 13 which is similar to case 15 but with a lower m_{om}.

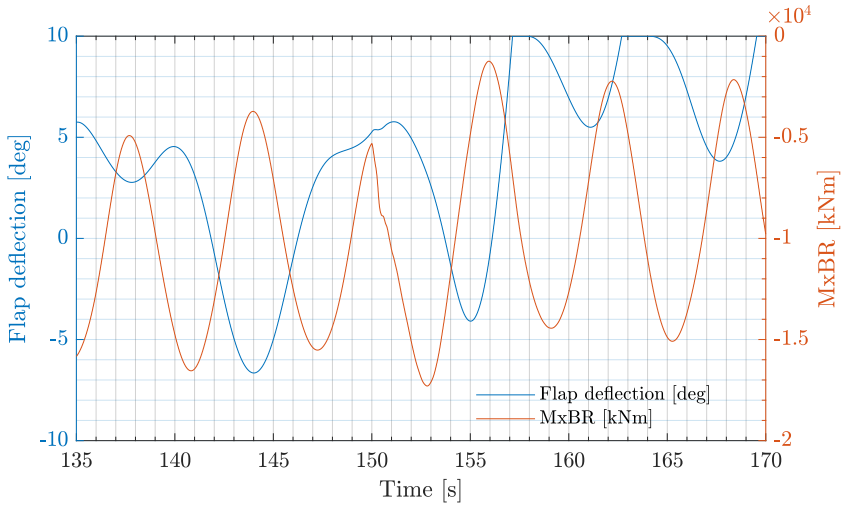

Figure 5.3: In this figure a step in wind speed from 20 to 22ms^{-1} was simulated at time =150s. The blade root flap-wise moment is shown for reference of the 1P frequency.

Analysis of blade root moments (MBR)

This section considers the analysis of the tuned flap. This part verifies that the flap behaves as expected and quantifies to what extent it alleviates loads. In these short simulations the standard deviation of the blade root moments are compared, following the naming convention used in the HAWC2 results. Following the blade root coordinate system in fig. 4.1: `MxBR` is the flap-wise blade root moment, `MyBR` the edge-wise blade root moment and `MzBR` is the torsional moment at the blade root. Posing that a lower standard deviation of the moments with a near similar mean would decrease lifetime damages, these values are compared to the baseline. In table 5.1 only wsp 22ms^{-1} is shown for comparison of two iterations. The first column shows the resulting reductions for case 13 and the second shows results for a later iteration of case 13. The later version has a reduced offset mass and lower spring stiffness than was considered in the table maker of chapter 4. Reducing the offset mass shows clear reductions in the edgewise vibrations which was the aim of changing this parameter. This however, reduces the inertial moment that is generated which gave cause for reduction of the spring stiffness as well.

For this last case the inertial moment acting on the flap and the flap angle can be seen in fig. 5.4. Here an increase of inertial moment (clockwise) results in a positive (clockwise) flap angle. There is a slight lag between the two due to inertial effects and the indicial response of the new flap position, influencing the aerodynamic moment and eventually the flap deflection. Furthermore, M_i oscillates around 700Nm which is nearly the value that the pre-load was tuned to. To estimate the pre-loads for a new case $M_{p,new}$, eq. (5.2)

Table 5.1: Reductions of the standard deviation of the root moments and the combined root moment. The middle column is case 13 as seen in the table and the last column is a later iteration of case 13. The reductions are for the wind speed of 22ms^{-1}.

Case	13	13 light
stdMxBR[%]	-4.43	-4.9
stdMyBR[%]	6.04	1.83
stdMzBR[%]	7.56	2.4
Combined[%]	9.18	-0.67

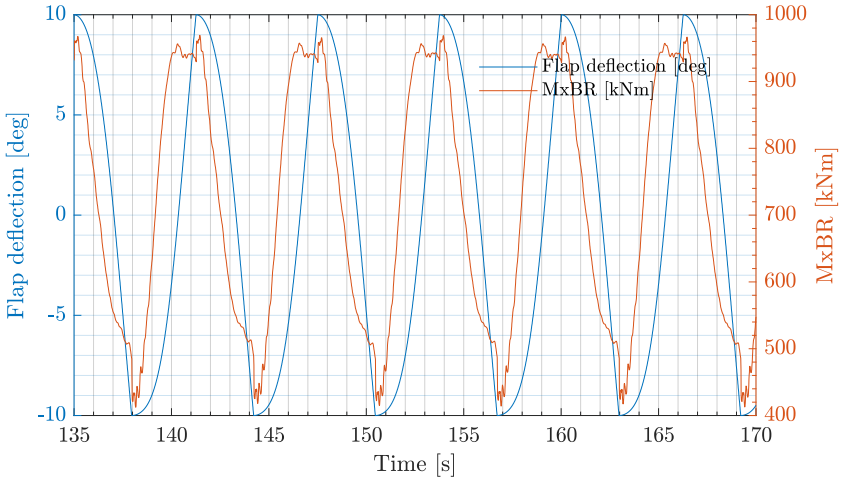

Figure 5.4: The inertial moment on blade one, Mi1 and the resulting flap angle delta on blade one.

was derived. Equation (5.2) relies on the assumption that the forcing moment on the flap is dominated by the inertial moment. Hereby assuming the blade accelerations stay similar, M_i changes only with m_{om} and d_{om}. This estimation saves much time when the pre-load values for an old case are known $M_{p,old}$.

$$M_{p,new} = \frac{M_{p,old}}{m_{om,old} d_{om,old}} \cdot m_{om,new} d_{om,new} \tag{5.2}$$

Tune remaining wind speeds and simulate with turbulence

The next two blocks are combined in this subsection, as they only need a brief explanation. If the preliminary simulation of the 22ms^{-1} case gives good results, the remaining wind speeds are tuned without turbulence, tower shadow and 200s simulations. With the correct pre-load now known for each wind speed, the next phase is to simulate with turbulence and for 700s. The first 100s of every the simulation are deleted to eliminate any initiation effects in the turbulent wind field. Adding turbulence in this last stage may result in nonzero mean flap deflections, due to gusts or jets but they are tuned correctly. The total distribution of M_p has been visualized in fig. 5.5, which shows that there are differences for the above rated wind speeds. The pre-load rapidly drops above rated. The cause of this can only be in the low-fidelity input to the MATLAB model. Gathering these statistics should have been done without turbulence to obtain more accurate values for in the steady MATLAB model.

Check the improvement in blade root moment

The penultimate stage is to compare the standard deviation of the blade root moments to those of the baseline model. The difference between the two root moments is given as a percentage. Besides the three blade root moments, the mean electrical power is considered in a similar fashion. If the decrease in loads has improved compared to other iterations or if a certain increase in loads is considered too high, a new case can be chosen and the process can start over again. The final resulting reductions compared to the baseline of case 13 and 3230 have been plotted in fig. 5.6. The suffix '30' of case 3230 indicates a 30% span flap. The red lines indicate the 10% flap and the blue lines indicate the 30% flap. The circle, cross and diamond each indicate a different root moment. The 30% flap yields the largest difference in root moments, the torsion moment

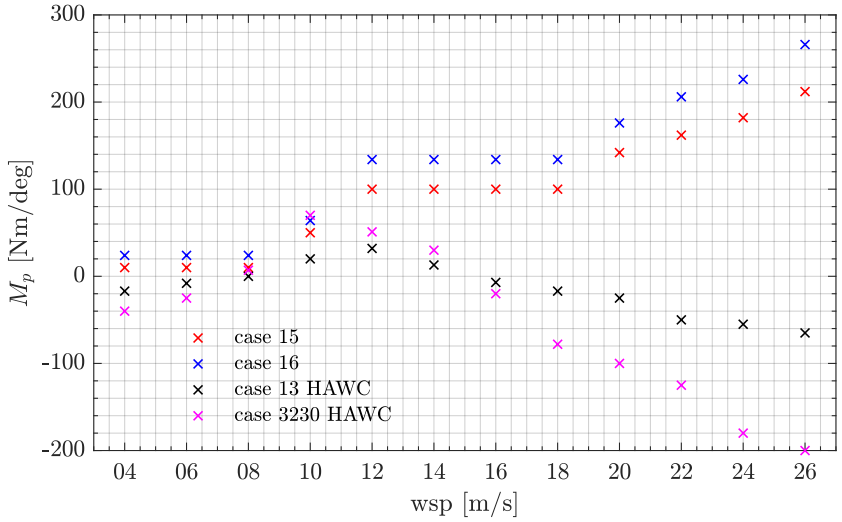

Figure 5.5: Comparison of M_p calculated in MATLAB and in HAWC2 for case 15, 16, 13 and 3230.

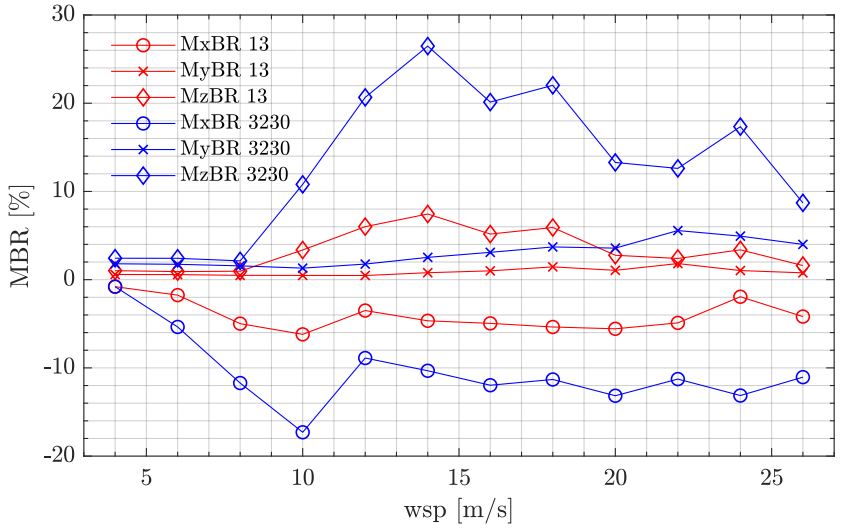

Figure 5.6: Resulting reductions of the standard deviation of the root moments after tuning case 13 (red) and case 3230 (blue).

increases drastically, just after rated. The flap-wise moments experience a peak in reductions at rated wind speed. The 10% flap yields milder differences in root moments. The trend for both lines is very similar. From this graph it appears that the previous goal of reducing edge-wise moments has been achieved but the torsion moments increase tremendously. However, with a flap that is three times as large one can also expect nearly three times as large torsion moments, because the flap drives this moment. The flap-wise reductions are satisfactory at this stage, causing cases 13 and 3230 to be used for the next part of the aeroelastic study.

Run full dlc1.2

Once all cases have been tuned and there is good reason to believe that a certain case results in reductions of the blade's lifetime loads, it is set up to run the complete dlc1.2. This includes the yaw miss-alignments and two turbulence seeds for each yaw direction. Then the effect can be seen on the lifetime equivalent loads and the distribution of loads for each wind speed. The findings are discussed in the results section, after it is explained how they were post-processed.

5.4. Post-processing

After the full design load case all the data must be post-processed using the designated software called Pdap (Python Data Analysis Program)[46], which is made for HAWC2 and written in Python. The software provides a powerful tool for evaluating data, equivalent loads, statistics, plotting the data and visualizing the power spectral density. For the dlc1.2, whose parameters were listed in table 3.4, a *standard report* listing statistics, minima, maxima and ultimately lifetime loads can be generated. Some methods in the Pdap software are explained in this section, namely, the calculation of the *Weibull* distribution to obtain the probability of each wind speed and direction occurring. These are important for the calculation of the weights necessary in the fatigue analysis, which will be discussed last.

5.4.1. Wind distribution and probability

Firstly, the wind distribution is generated from the *Weibull* parameters which are fixed for the dlc1.2. These parameters originate from the wind turbine IEC class IA, for which the reference wind speed is V_{ref}=50ms^{-1}. The reference wind speed u_{ref}=0.2*V_{ref}, for this calculation. The wind speed ranges from 4 to 26ms^{-1}, in *steps* of 2ms^{-1}. Then, using eq. (5.3), the probability of occurrence of each wind speed can be calculated. For each wind speed two yaw misalignments are calculated, besides the zero yaw angle. The zero yaw occurs 50% of the time and the two yaw cases occur 25% of the time each, which is representative of the probability of each wind direction $wdir$.

$$P(wsp) = e^{-\left(\frac{wsp-\frac{step}{2}}{\frac{2u_{ref}}{\sqrt{\pi}}}\right)^2} - e^{-\left(\frac{wsp+\frac{step}{2}}{\frac{2u_{ref}}{\sqrt{\pi}}}\right)^2} \tag{5.3}$$

5.4.2. Fatigue Analysis

The first step in fatigue analysis, consists of rain flow counting done on a signal. Here the range S_i of each change in load is counted as one cycle. Using the total amount of cycles N_i at each range, the Palmgren-Miner states that summing the product of these two can be taken to find the total amount of damages. However, the higher amplitudes do more damage than the low stress changes, which follows the slope of the Wöhler curve given by parameter m. For steel structures like the tower and for the composite blades, m is 4 and 10 respectively. Now, the short term equivalent load, $stel$, is calculated as in eq. (5.4) with N_{eq} the total length of the simulation in seconds, which is 600s.

$$stel = \left(\frac{(\sum_i N_i S_i^m)}{N_{eq}}\right)^{m^{-1}} \tag{5.4}$$

From the short term equivalent loads, the lifetime load L_{eq} can be calculated using eq. (5.5). A wind turbine lifetime is 20 years, normally estimated as N_{eqL}=1E7s. In the case of the lifetime loads for blades, one should not forget that N_{eq} is 3x600s accounting for all blades.

$$L_{eq} = \left(\frac{(\sum stel^m N_{eq} weight)}{N_{eqL}}\right)^{m^{-1}} \tag{5.5}$$

The $weight$ used above defines how often a results file is accounted for in its lifetime of 20 years. Multiplying the probability of a wind speed with that of a dlc and that of a wind direction results in eq. (5.6).

$$P(case) = P(dlc) \cdot P(wsp) \cdot P(wdir) \tag{5.6}$$

In eq. (5.7) the amount of hours in 20 years of this case can be calculated.

$$Hours(case) = P(case) \cdot \frac{hours}{20 years} \tag{5.7}$$

Finally, the $weight$ can be calculated as in eq. (5.8). Here, the length of the case is the 600 seconds. There are 3600 seconds per hour and there are six files per case.

$$weight(case) = Hours(case) \frac{sec/hour}{length(case) length(files)} = Hours(case) \frac{3600}{600 \cdot 6} \tag{5.8}$$

5.5. Results & Discussion

The results from the simulations are presented below. Two major cases are considered, namely, case 13 and case 3230, which is a 10% flap and a 30% flap, respectively. Results consider the lifetime equivalent load and extreme loads compared to the baseline model. Some cases that were tried but did not show enough potential to simulate dlc1.2, will be discussed briefly at the end of this section. The two main cases have the flap parameters listed below in table 5.2. The added mass due to the offset mass is 84kg and 255kg per blade for case 13 and 3230, respectively. The distance of the offset mass is .15m to the hinge. This ensures a low inertia so the flap reacts swiftly but still enough mass to react to the blade vibrations.

Table 5.2: The five flap parameters corresponding to cases 13 and 3230 that are referred to in the results.

Case	$\mathbf{K_f}$[Nm deg^{-1}]	$\mathbf{m_{om}}$[%]	$\mathbf{d_{om}}$[%]	**span**[**r**/**R**]	$\mathbf{c_f}$[%]
13	3	5	4	[0.7 0.8]	10
3230	10	5	4	[0.6 0.9]	10

The output of Pdap is a list of measured values at the various sensor points. Each sensor point is named with the abbreviations used below:

- *MxTB*: Moment at the Tower Bottom around the x-axis resulting in a fore-aft (FA) motion.
- *MyTB*: Moment at the Tower Bottom around the y-axis resulting in a side-side (SS) motion.
- *MxTT*: Moment at the Tower Top around the x-axis resulting in tilt.
- *MyTT*: Moment at the Tower Top around the y-axis resulting in roll.
- *MzTT*: Moment at the Tower Top around the z-axis resulting in yaw.
- *MxMB*: Moment at the Main Bearing around the x-axis resulting in tilt.
- *MyMB*: Moment at the Main Bearing around the y-axis resulting in yaw.
- *MzMB*: Moment at the Main Bearing around the z-axis resulting in torsion.
- *MxBR*: Moment at the Blade Root around the x-axis also referred to as flap-wise moment.
- *MyBR*: Moment at the Blade Root around the y-axis also referred to as edge-wise moemnt.
- *MzBR*: Moment at the Blade Root around the z-axis also referred to as torsion moment.

A first look at the flap deflection statistics gives insight in the working principle. From fig. 5.7 the mean flap deflection is close to zero, which was the aim of the tuning. In general the mean deflection was tuned to be within a half a degree of zero. For the wind speed of 20ms^{-1} the pre-tension seems improperly tuned resulting in a positive flap angle of 2 degrees. This error can only be attributed to human error, when implementing the pre-tension of the spring. The effect of this is increased loads, because the positive deflection increases the aerodynamic force on the blade, where the blade pitching mechanism is trying to reduce loads. The trend of the standard deviation resembles the power curve, which increases with rotational speed and relative velocity and becomes constant at rated. The higher standard deviation above rated, indicates high flap activity in this region, where fatigue takes most toll. With increased rotational speed and turbulence at above rated wind speeds, the blade vibrations are highest here. Being the main driving force for the flap this results in high flap activity. The spread of flap deflections appears to be highest near rated, where the rotational speed of the turbine is still varying and pitching starts to activate.

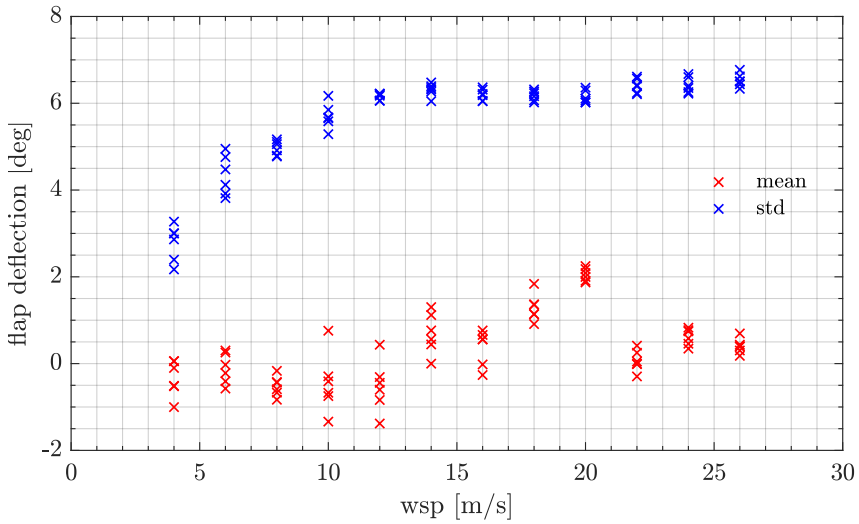

Figure 5.7: Statistics on the deflection of one flap for all six wind directions per wind speed for the 10% flap.

The reduced blade loads are also visible when the power spectral density is considered in fig. 5.8. The baseline is compared to the 10% and 30% flap at a wsp of 20ms^{-1}. At this rotational speed the 1P frequency is 0.16Hz. The magnitude of the peak at 1P is tremendous, compared to neighboring frequencies and is attenuated considerably by the flaps. Following intuition, the larger flap is visibly more able to attenuate blade root moments. The flap proves capable of reducing loads in the 1P frequency range.

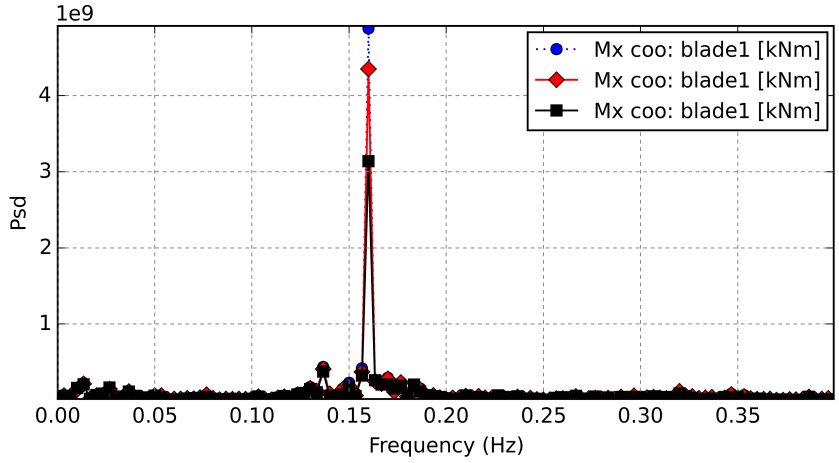

Figure 5.8: The psd of the blade root moments of the baseline (blue), 10% (red) and 30% (black) flap. The frequency that is visible for this 20ms^{-1} case is the 1P frequency at 0.16Hz.

5.5.1. Distribution of *stel*

The short term equivalent loads give information on how much a specific load is reduced. In the fig. 5.9 the *stel* for MxBR case 13 can be seen. At every wind speed, it results in a reduction compared to the baseline model. The trend of short term equivalent loads does not change its distribution of the *stel*. The incorrect tuning of the pre-load that was visible at 20ms^{-1} in fig. 5.7 does not have any noticeable consequence on the *stel*.

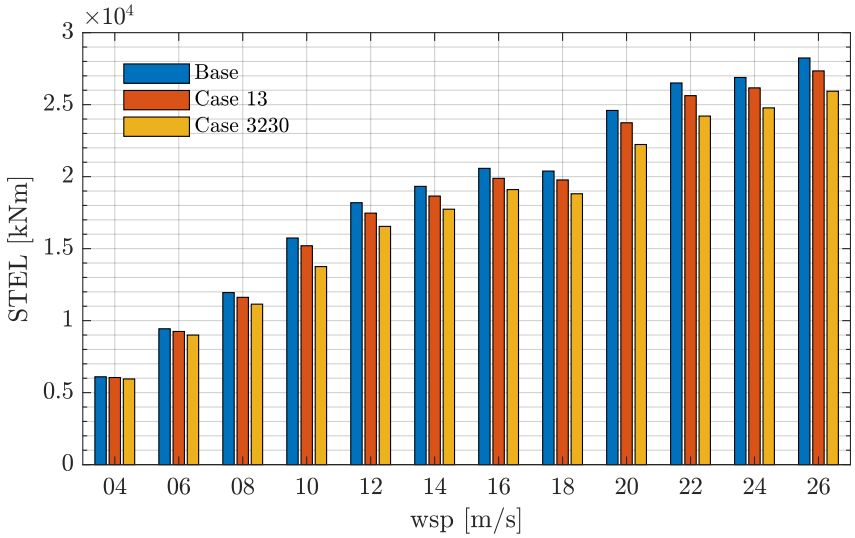

Figure 5.9: Mean short term equivalent load of MxBR for each wind speed.

5.5.2. Lifetime Equivalent Loads

Below the resulting lifetime equivalent loads are presented. Starting with the blade root moments as they are the primary goal of this study. The MxBR reduces by several percent. As comparison, an active flap with similar span and chord as the case 3230 is used in research from T. Barlas et al. 2016 [47], which achieved 12.1% reduction. Achieving 72% of the reduction the active method achieves with the robust semi-passive design is a satisfactory result. The increase in MyBR is expected, as the edgewise vibration is dominated by gravity and the system adds mass to the blades resulting in higher loads. Reducing these loads was the goal of choosing a light offset mass. The MzBR increases as well, due to the pitching moment a flap creates. For the larger span this increase is considerable. The bearing loads are discussed in the next subsection. The tower top experiences reductions in moments around all three axes. It is peculiar that the tower top loads reduce, where they increase at the tower bottom.

This is so, because of the extra added mass on the blade, inducing a fore-aft motion. The rotor tilt causes the added weight to displace fore-aft. In comparison to the 10% flap from Montinari, there are several differences. Whereas it has a similar span, the chord of the flap is 25% blade chord; overhang of 53%; the offset mass is 18% of the sectional mass; the offset distance is 21% of the blade chord. Concluding that these are two largely different flaps, simulated on the same turbine. The effect of a heavier mass is instantly visible in the edgewise lifetime loads. The larger flap chord does achieve nearly twice as much alleviation of the flap-wise loads, compared to the 10% flap in the current study. Finally, a larger flap chord results in increased torsion moments. Case 13 of the present study achieves much milder negative effects on the blade, which can be desirable depending on the application. However, comparing the 10% flap of Montinari with the 30% flap of this thesis seem more adequate as they add nearly the same amount of mass to the blade and achieve similar lifetime loads. The question is raised on how feasible the implementation of Montinari's 10% flap is considering the size of flap chord, offset mass distance and added mass, which must operate inside the blade structure. Similarly, the 30% flap span results in other implementation problems.

Table 5.3: The lifetime equivalent loads of the two cases given as a percentage of change with respect to the baseline.

Sensor	Case 13 [%]	Case 3230 [%]
MxTB	0.4	13.9
MyTB	1.9	6.1
MxTT	-2.4	-4.1
MyTT	-1.5	-2.6
MzTT	-2.7	-3.5
MxMB	-3.2	-6
MyMB	-3.4	-6.3
MzMB	14.5	-44.3
MxBR	-3.4	-8.7
MyBR	0.4	1.8
MzBR	0.6	9

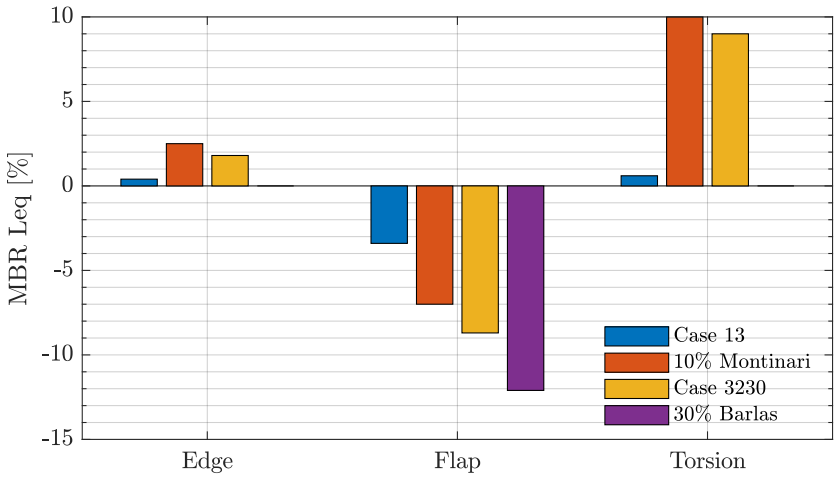

Figure 5.10: Comparison of the Weibull Weighted DEL for the present study with work from Montinari 2019 [35] and work from Barlas (2016) [47].

5.5.3. Drive-train mode

Besides the clear decrease in loads on the main bearing an increase is also visible at the MzMB for the 10% flap and a reduction during case 3230. MzMB considers torsion experienced by the rotor shaft which can have an interaction with edgewise modes of the blades. During the course Loads Aerodynamics and Control (LAC) a similar problem was encountered when up-scaling the rotor blade, which, similar to this research, increases the blade mass. The drive-train however, is not designed to withstand such torsion. When designing a heavier rotor a stronger shaft should be present. Using HAWCStab2, a frequency domain tool which is used to calculate structural and aeroelastic modes of HAWC2 models, one can visualize modal vibrations. The program can visualize and exaggerate blade and turbine modes, while yielding their respective frequencies. For the combined edge-wise and shaft mode the modal frequency is 3.4Hz. Regarding the power spectral density of MzMB (blue) in fig. 5.11, a clear peak is visible around this frequency. As mentioned, this problem can be solved by designing a stiffer shaft or scheduling the control gains properly again. The controller uses a filter which is limited to a certain frequency, however, this frequency now drops due to the increased mass of the blade. This could prohibit the controller functioning correctly. A simple solution is to increase the drive-train shaft material stiffness, resulting in the red line in fig. 5.11. A clear reduction of the 3.4Hz peak is visible after increasing the stiffness and the peak shifts slightly to higher frequencies. This was done for case 3230 which results in the lifetime loads of MzMB reducing by -44.3%. For case 13 the lifetime simulation was not done with the stiff shaft, which is the reason it shows the large increase in lifetime loads for MzMB.

5.5.4. Ultimate Loads

Reducing ultimate loads is also a great benefit of flaps. Quantifying the effect the two flap cases have on ultimate loads is the goal of this section. The Weibull weighted ultimate loads are shown in fig. 5.12. The out-of-plane ultimate load reduce by 1.7% and 2.3% for the small and large flap respectively. The in-plane-loads increase for the small flap by 0.75% and decrease for the large flap by 0.79%. This is a result of the stiff shaft that was used to simulate the large flap, reducing the edgewise mode of the blade. The torsion mode increases by 12.3% for the large flap and merely 0.13% for the 10% flap. Regarding the distribution of the torsion moments in fig. 5.13, they greatly increase above rated where the flap has highest activity, as seen in fig. 5.7. This increased activity results in these torsion moments.

The differences in MxBR are given as a percentage compared to the baseline in fig. 5.14. For al wind speeds the flaps result in lower ultimate loads. There are some differences in the distribution of the ultimate load reduction. The largest reduction for the large flap is at $10ms^{-1}$ and for the small flap this is at $12ms^{-1}$. Also for both cases there is an increase in reduction at $22ms^{-1}$. Finally, Pdap outputs tables listing the minimum and maximum value for each of the sensors and to which dlc it belongs. The tables are added in appendix C in appendix C. It is shown that the 10% flap increases tower loads and decreases bearing ultimate loads. Also the blade root ultimate load decreases in the flap-wise and edge-wise direction. The ultimate distance from the blade tip reduces minimally. For the 30% flap the ultimate loads are reduced for the blade flap-wise moments.

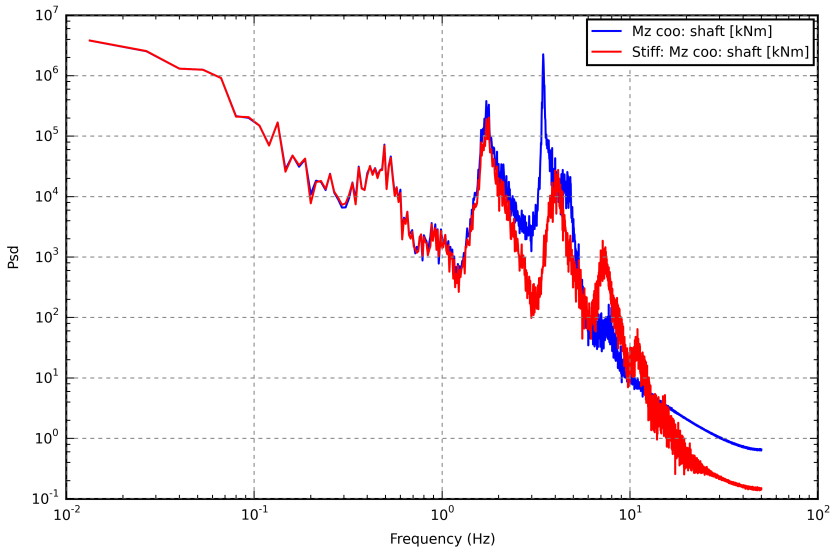

Figure 5.11: Power spectral density of MzMB with a regular drive-train shaft (blue) and stiff shaft (red).

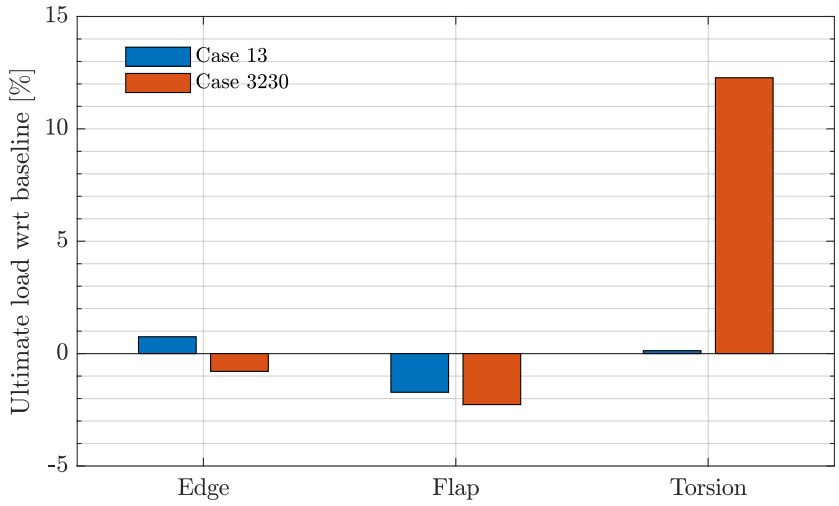

Figure 5.12: Weibull weighted ultimate load reduction of MxBR, MyBR and MzBR with respect to the baseline model for the 10% flap and the 30% flap.

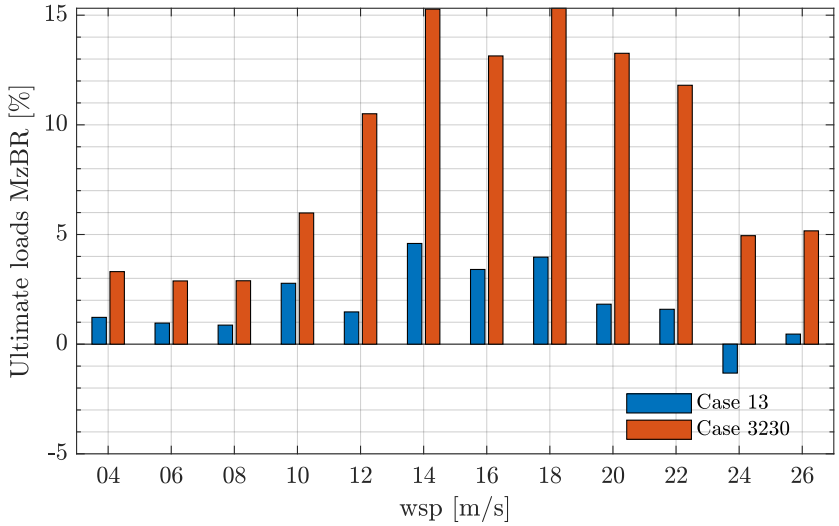

Figure 5.13: The distribution of the ultimate torsion moments acting on the blade root for case 13 and case 3230.

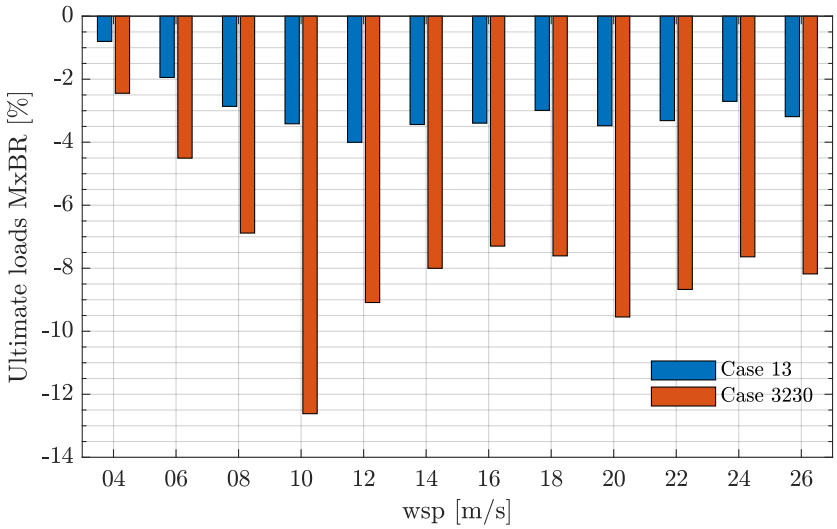

Figure 5.14: The distribution of the MxBR ultimate loads per wind speed for the small and the large flap.

MxTB increases, whereas MyTB decreases. The tower top loads all decrease and the main bearing loads are disregarded as it it simulated with the stiff shaft. A minimal increase is visible for tip clearance.

5.5.5. Annual Energy Production

The use of flaps on a turbine can decrease the annual energy production when placed on a reference turbine. An increase in AEP can be achieved by increasing the turbine size while keeping the loads similar to the original model by adding load reducing flaps. The AEP was calculated using the probability derived in eqs. (5.3) and (5.6). The probabilities for these wind speeds are multiplied with the average of the corresponding electrical power output. Summing up the weighted power and multiplying it by the amount of seconds per year, denoted by *time*, following eq. (5.9). In comparison to the baseline the 10% flap loses 0.26% power and the 30% flap loses 0.45% power. The source of this problem becomes evident in fig. 5.15, where the below rated power production deviates from the case without flap. Non-zero mean flap deflections and high flap activity causes for sub-optimal behavior of the airfoil, where it is supposed to operate most efficiently. Tuning the hinge spring pre-tension more accurately could reduce these losses as well. Moreover, the reductions are very low and the benefits in AEP should be analyzed in terms of an increased turbine size. The losses above rated are so low that they are not visible in the graph which is a satisfactory result.

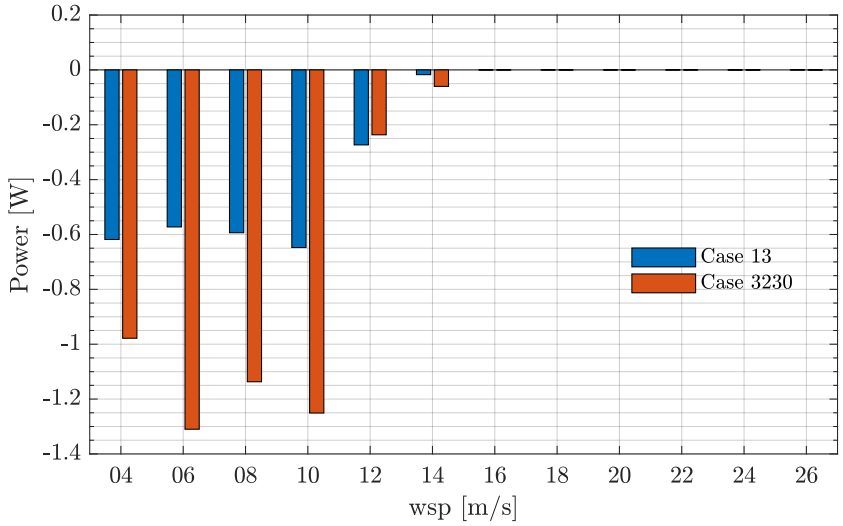

Figure 5.15: The difference in power production with respect to the baseline per wind speed for the 10% and 30% flap.

$$AEP = time \cdot \sum_{wsp} P_{wsp}(case) \cdot Power_{wsp} \tag{5.9}$$

5.5.6. Comparison of other spanwise distributions

Many different parameter combinations were studied, the most successful were discussed previously. However, some different span-wise distribution were considered in terms of the blade root standard deviations as in the last steps of fig. 5.2. For instance two varieties of case 13 were considered with a 20% span from [0.6 0.8]$\cdot R$ and with a 10% span at span-wise position [0.8 0.9]$\cdot R$. At this stage the offset mass was still at 30% of the blade mass and a midway solution was sought after between the 10% and 30% flap previously discussed. The 10% flap placed further along the blade was named case 1389 and the 20% flap is named case 1320. The 20% flap indeed resulted in a mid-way between the 10 and 30% flap so it was not further investigated. The 10% flap increased the edgewise root moments, such, that it was also abandoned from further investigation.

5.6. Conclusions

All the aeroelastic simulations are satisfactory to the extent of this research. The implementation of the `.dll` took longer than expected, due to the lack of knowledge of the programming language the author had of Fortran. That said, troubleshooting is difficult when running HAWC2 and the Fortran `.dll` through MATLAB. Especially due to the extensive duration of time needed for a simulation. The pre-load tuning scheme was formulated and successfully carried out. Simulating the dlc1.2 simulations took nearly a day per case. Using the post processing program, Pdap, saved much time while looking through the produced data and helped to form conclusions but does not have much options in terms of plotting. The aeroelastic model allowed to compare the flap to the baseline model, in answer to the second research question. The answer was split into sub-questions comparing fatigue loads, AEP and ultimate loads, which is summarized below. The last research question was to compare to other models which is visible in fig. 5.10.

- Lifetime load reductions of 8.7% for MxBR and 6% at main bearing yaw and tilt which is only 25% less than can be achieved in active solutions [47].
- Tower top lifetime equivalent loads reduce and tower bottom loads increase for both flap systems.
- An increase in MyBR and MzBR lifetime equivalent loads of 1.8% and 9%, respectively, for the 30% span flap, which is expected with the current mechanism. For the 10% flap, MyBR and MzBR lifetime equivalent loads only increase by 0.4 and 0.6%, respectively.
- A combined edge-wise and drive-train torsion mode was present due to the increased weight of the

blades and drive-train shaft not being stiff enough. This combined mode increases main bearing torsion lifetime loads.

- Ultimate MxBR loads are reduced by -1.7% and -2.27% for the 10% and 30% flap, respectively.
- AEP losses are limited to 0.26 and 0.45% for the small and large flap, respectively.
- Pre-loads are different from those calculated by the analytical solutions from chapter 4. The source is at the low-fidelity input as the models are otherwise identical. Modeling this better could eliminate the time necessary to tune the pre-tension in HAWC2, allowing for the analysis of more cases.
- Research should be done on increasing the turbine size at similar loads and quantify the AEP increase.

6 Conclusions

DRIVEN by the incentive to become more competitive to energy solutions, relying on fossil fuels wind energy technology is making great progress. One of these leaps is the concept of 'smart' rotors to enable increasing the turbine size. This thesis proves a semi-passive trailing-edge flap concept, built on work from Pierluigi Montinari et al. [35] and Carlo L. Bottasso et al. [33]. The research clearly achieves reductions in the flap-wise bending moments, which can result in a cheaper blade. Besides cheaper blades, it can result in a larger blade, capturing more energy and reducing the cost of energy. Many might find that 'smart' rotors are too complex to be implemented on wind turbines, however, the same was thought of individual pitch control some time ago. This research is only preliminary; more research should be done on increasing turbine size in combination with the semi-passive flap.

6.1. Mathematical Model

The mathematical model was discussed in chapter 4 and was used to develop and test the reaction of the flap to blade vibrations. During this fast, low-fidelity study, many flap parameters were combined, resulting in a ranking of its load alleviating potential. The first research question and its sub-questions were answered in this section.

6.1.1. Conclusions

The first research question was how the pre-load of the mechanism varies with wind speed. An estimate was found in fig. 4.9, which was not accurate for higher wind speeds and follows a different distribution. The sub-questions used to answer this research question were to find the input parameters for the model and their distribution from cut-in to cut-out wind speed. These were found for the angle of attack, relative velocity, rotational speed, blade accelerations and blade orientation. Their respective distributions are shown in figs. 4.2 to 4.7. The last sub-question was to constrain the parameters of the flap, which was done in table 3.1. All these questions lead to the implementation of the model and the following conclusions:

- Desirable flap behavior was accomplished and the flap response is as intended.
- Rotation of the driving servo motor to achieve pre-load must have high precision or a transmission might be necessary. This reduces robustness of the system. The higher the load authority of the flap, the higher the actuator rotation.
- The flap with the highest load alleviation potential uses a high mass close to the flap hinge. The greatest driving moment can be achieved by increase the offset mass and its distance to the hinge however, then the inertia increases as well. This is the main trade-off.

6.1.2. Recommendations

Some recommendations for improving this model:

- The resulting table does not account for damages that will occur from the increased mass. Finding a range for these damages in HAWC2 and iterating back to MATLAB, one could set a limit to the increased mass.

- Modeling the input more accurately could lead to more exact results, that agree more with HAWC2 results. For instance, feeding data from the HAWC2 time simulations in as input could solve this, improving the pre-load estimation.

6.2. Aeroelastic Model

After implementing the flap into the aeroelastic model, described in chapter 5, the aeroelastic response of the flap and ultimately the lifetime loads can be quantified. This answers the last two research questions.

6.2.1. Conclusions

The second research question was to compare the flap model with the baseline DTU10 MW wind turbine in terms of AEP, lifetime fatigue and ultimate loads. The last research question was to compare the model to other existing load alleviation methods. Answers to the research questions and more are summarized below:

- The pre-loads in HAWC2 differ from those calculated in MATLAB, in chapter 4. The difference in distribution can seen in fig. 5.5. The cause is most likely at the static input to the model. Improving the model in this aspect could eliminate tuning the pre-load in HAWC2, saving time.
- Lifetime reductions, shown in table 5.3, of 8.7% for MxBR and 6% at main bearing yaw and tilt, have been achieved with the 30% flap. This is 25% less than an active solution on the same turbine with similar span and chord. The comparison is visible in fig. 5.10.
- Tower top loads reduce and tower bottom loads increase compared to the baseline.
- Increase in MyBR and MzBR of 1.8% and 9%, respectively, which is expected for the large flap. The small flap only experienced 0.4% and 0.9% increase in edge-wise and torsion moments at the blade root.
- A combined edge-wise and drive-train torsion mode was present due to the increased weight of the blades and drive-train shaft not being stiff enough. This combined mode increases shaft torsion lifetime loads.
- Ultimate MxBR loads are reduced by -1.7% and -2.27% for the 10% and 30% flap respectively.

6.2.2. Recommendations

Although the conclusions are well supported by the simulations of the current study, I recommend research in the following direction:

- Running a full design load basis (DLB) should be done, to find the reaction of the flap in e.g. parked situation or grid failure.
- Quantifying the possible increased turbine size and corresponding AEP increase. This allows to calculate the effect on the levelized cost of energy (LCOE).
- The control of the pre-tension is now scheduled with mean wind speed, a more realistic control should be be implemented in the DTU controller.
- A wind tunnel experiment should be set up to verify the behavior on an airfoil.

Bibliography

[1] P. T. Iván Pineda. Wind in power annual 2017: combined onshore and offshore wind energy statistics. Report, Wind Europe, 2018.

[2] R. 2018. Renewables 2018 global status report. Report, Paris: REN21 Secretariat, 2018.

[3] G. Sieros, P. Chaviaropoulos, J. D. Sørensen, B. H. Bulder, and P. Jamieson. Upscaling wind turbines: theoretical and practical aspects and their impact on the cost of energy. *Wind Energy*, 15(1):3–17, 2012. ISSN 10954244. doi: 10.1002/we.527.

[4] G. Galilei. Discorsi e dimostrazioni matematiche intorno a due nuove scienze (leiden, 1638); trans. *H. Crew and A. de Salvio as Dialogues Concerning Two New Sciences*, page 2, 1914.

[5] T. K. Barlas and G. A. M. van Kuik. Review of state of the art in smart rotor control research for wind turbines. *Progress in Aerospace Sciences*, 46(1):1–27, 2010. ISSN 03760421. doi: 10.1016/j.paerosci.2009.08.002.

[6] Z. J. Chen, K. A. Stol, and B. R. Mace. Wind turbine blade optimisation with individual pitch and trailing edge flap control. *Renewable Energy*, 103:750–765, 2017. ISSN 09601481. doi: 10.1016/j.renene.2016.11.009.

[7] D. Yen, C. van Dam, R. Smith, and S. Collins. Active load control for wind turbine blades using mem translational tabs. *20th 2001 ASME Wind Energy Symposium*, 2001. doi: 10.2514/6.2001-31.

[8] M. K. McWilliam, T. K. Barlas, H. A. Madsen, and F. Zahle. Aero-elastic wind turbine design with active flaps for aep maximization. *Wind Energy Science*, 3(1):231–241, 2018. ISSN 2366-7451. doi: 10.5194/wes-3-231-2018.

[9] F. Z. Christian Bak, R. Bitsche, T. Kim, A. Yde, L. C. Henriksen, A. Natarajan, and M. H. Hansen. Description of the dtu 10 mw reference wind turbine. Report, DTU, 2013.

[10] W. M. J. Jonkman, S. Butterfield and G. Scott. Definition of a 5-mw reference wind turbine for offshore system development. Report, NREL, 2009.

[11] M. L. Corradini, G. Ippoliti, and G. Orlando. Observer based blade-pitch control of wind turbines operating above rated: a preliminary study. *IFAC-PapersOnLine*, 50(1):9914–9919, 2017. ISSN 24058963. doi: 10.1016/j.ifacol.2017.08.1631.

[12] E. A. Bossanyi. Further load reductions with individual pitch control. *Wind Energy*, 8(4):481–485, 2005. ISSN 1095-4244 1099-1824. doi: 10.1002/we.166.

[13] S. C. Thomsen, H. Niemann, and N. K. Poulsen. Individual pitch control of wind turbines using local inflow measurements. *IFAC Proceedings Volumes*, 41(2):5587–5592, 2008. ISSN 14746670. doi: 10.3182/20080706-5-kr-1001.00942.

[14] T. Barlas, J. W. van Wingerden, A. Hulskamp, and G. van Kuik. Closed-loop control wind tunnel tests on an adaptive wind turbine blade for load reduction. *46th AIAA Aerospace Sciences Meeting and Exhibit*, 2008. doi: 10.2514/6.2008-1318.

[15] T. L. A. Helge Aagaard Madsen, Thanasis Barlas. A morphing trailing edge device for a wind turbine. In *7th ECCOMAS Thematic Conference on Smart Structures and Materials*, pages 691–701, 2015. ISBN 1045-389X 1530-8138.

[16] N.-C. Oltmann, D. Sobotta, and A. Hoffmann. Load reduction of wind turbines using trailing edge flaps. *Energy Procedia*, 136:176–181, 2017. ISSN 18766102. doi: 10.1016/j.egypro.2017.10.316.

[17] E. S. Carrolo. *Passive Control of Aerodynamic Load in Wind Turbine Blades*. Thesis, Técnico Lisboa, 2015.

[18] T. Bagherpour, X. M. Li, D. I. Manolas, and V. A. Riziotis. Modeling of material bend-twist coupling on wind turbine blades. *Composite Structures*, 193:237–246, 2018. ISSN 02638223. doi: 10.1016/j.compstruct.2018.03.071.

[19] D. I. Manolas, G. P. Serafeim, P. K. Chaviaropoulos, V. A. Riziotis, and S. G. Voutsinas. Assessment of load reduction capabilities using passive and active control methods on a 10mw-scale wind turbine. *Journal of Physics: Conference Series*, 1037, 2018. ISSN 1742-6588 1742-6596. doi: 10.1088/1742-6596/1037/3/032042.

[20] P. Bortolotti, C. L. Bottasso, A. Croce, and L. Sartori. Integration of multiple passive load mitigation technologies by automated design optimization-the case study of a medium-size onshore wind turbine. *Wind Energy*, 22(1):65–79, 2019. ISSN 10954244. doi: 10.1002/we.2270.

[21] S. C. Doney, P. Test of a gust-alleviating flap in the gust tunnel. Report, NACA, 1940.

[22] R. H. Stroub. An analytical investigation of the free-tiprotorfor helicopters. Report, Technical Memorandum 81345, 1982. URL `https://ntrs.nasa.gov/search.jsp?R=19820010305`.

[23] G. A. M. van Kuik and J. W. M. Dekker. The flexhat program, technology development and testing of flexible rotor systems with fast passive pitch control. *Journal of Wind Engineering and Industrial Aerodynamics*, 39(1-3):435–448, 1992. ISSN 01676105. doi: 10.1016/0167-6105(92)90567-t.

[24] C. L. Bottasso, A. Croce, F. Gualdoni, P. Montinari, and C. E. D. Riboldi. Articulated blade tip devices for load alleviation on wind turbines. *Wind Energy Science*, 1(2):297–310, 2016. ISSN 2366-7451. doi: 10.5194/wes-1-297-2016.

[25] U. Cordes, B. Lambie, K. Hufnagel, H. Spiegelberg, G. Kampers, and C. Tropea. The adaptive camber concept-a passive approach for gust load alleviation on wind turbines. *Wind Energy*, 21(9):732–744, 2018. ISSN 10954244. doi: 10.1002/we.2190.

[26] B. Lambie. *Aeroelastic Investigation of a Wind Turbine Airfoil with Self-Adaptive Camber*. Thesis, Technischen Universität Darmstadt, 2011.

[27] B. Lambie, M. Jain, C. Tropea, and G. Spelsberg-Korspeter. Passive camber change for windturbine load alleviation. *49th AIAA Aerospace Sciences Meeting including the New Horizons Forum and Aerospace Exposition*, 2011. doi: 10.2514/6.2011-637.

[28] L. O. Bernhammer, S. T. Navalkar, J. Sodja, R. De Breuker, and M. Karpel. Experimental investigation of an autonomous flap for load alleviation. *56th AIAA/ASCE/AHS/ASC Structures, Structural Dynamics, and Materials Conference*, 2015. doi: 10.2514/6.2015-1852.

[29] S. T. Navalkar, L. O. Bernhammer, J. Sodja, C. J. Slinkman, J. W. van Wingerden, and G. A. M. van Kuik. Aeroelastic design and lpv modelling of an experimental wind turbine blade equipped with free-floating flaps. *Journal of Physics: Conference Series*, 753, 2016. ISSN 1742-6588 1742-6596. doi: 10.1088/1742-6596/753/4/042010.

[30] L. O. Bernhammer, S. T. Navalkar, J. Sodja, R. D. Breuker, and M. Karpel. Experimental and numerical investigation of an autonomous flap for load alleviation. *Journal of Aircraft*, 54(2):464–475, 2017. ISSN 0021-8669 1533-3868. doi: 10.2514/1.C033767.

[31] G. G. L. V. Pierluigi Montinari, Carlo L. Bottasso. *Blade Passive Solutions for Load Mitigation on Multi-Megawatt Wind Turbines*. Thesis, Politecnico di Milano, 2017.

[32] C. L. Bottasso, A. Croce, F. Gualdoni, and P. Montinari. A new concept to mitigate loads for wind turbines based on a passive flap. *2015 American Control Conference (Acc)*, pages 3066–3069, 2015. ISSN 0743-1619. doi: ACC.2015.7171803. URL `<GotoISI>://WOS:000370259203026`.

[33] C. L. Bottasso, A. Croce, F. Gualdoni, and P. Montinari. Load mitigation for wind turbines by a passive aeroelastic device. *Journal of Wind Engineering and Industrial Aerodynamics*, 148:57–69, 2016. ISSN 01676105. doi: 10.1016/j.jweia.2015.11.001.

[34] F. G. Carlo L. Bottasso, Alessandro Croce. New concepts to control the load along the span of the blade, passive, active or mixed. Report, INNWIND, 2015.

[35] P. Montinari, F. Gualdoni, A. Croce, and C. L. Bottasso. Ultimate and fatigue load mitigation by an inertial-driven passive flap, using a geometrically exact multibody formulation. *Journal of Wind Engineering and Industrial Aerodynamics*, 175:169–178, 2018. ISSN 0167-6105. doi: 10.1016/j.jweia.2018.01.038. URL <GotoISI>://WOS:000430758700015.

[36] T. Barlas, V. Pettas, D. Gertz, and H. A. Madsen. Extreme load alleviation using industrial implementation of active trailing edge flaps in a full design load basis. *Journal of Physics: Conference Series*, 753, 2016. ISSN 1742-6588 1742-6596. doi: 10.1088/1742-6596/753/4/042001.

[37] A. M. Larsen, Torben J.; Hansen. How 2 hawc2, the user's manual,ver. 4-7. Report 0106-2840, DTU Wind Energy, 2007 2007.

[38] M. Bergami, Leonardo; Gaunaa. Ateflap aerodynamic model, a dynamic stall model including the effects of trailing edge flap deflection. Report, DTU Wind Energy, 2012.

[39] A. N. Morten Hartvig Hansen, Kenneth Thomsen. Design load basis for onshore turbines. Report, DTU Wind Energy,DTU Wind Energy E, No. 0074(EN), 2015.

[40] H. Blasius. The boundary layer in fluids with little friction. *NACA*, 1908.

[41] D. C. Bratton and C. A. Womeldorf. The wind shear exponent: Comparing measured against simulated values and analyzing the phenomena that affect the wind shear. *ASME 2011 5th International Conference on Energy Sustainability, Parts A, B, and C*, pages 2245–2251, 2011. doi: DOI:10.1115/es2011-54823.

[42] S. B. Pope. *Turbulent Flows*. Cambridge University Press, 2000. ISBN 9780521598866.

[43] A. Chougule, J. Mann, M. Kelly, and G. C. Larsen. Modeling atmospheric turbulence via rapid distortion theory: Spectral tensor of velocity and buoyancy. *Journal of the Atmospheric Sciences*, 74(4):949–974, 2017. ISSN 0022-4928 1520-0469. doi: 10.1175/jas-d-16-0215.1.

[44] T. Beddoes. Practical computations of unsteady lift. *Vertica*, 8(1):55–71, 1984.

[45] K. N. M.H. Hansen. A beddoes-leishman type dyanmic stall model in state-space and indicial formulations. *Technical Report R-1354(EN)*, 2004.

[46] Pedersen and M. Mølgaard. Post processing of design load cases using pdap. *DTU Wind Energy*, I(No. 0371), 2014.

[47] F. Z. H. M. Thanasis K. Barlas, Carlo Tibaldi. Aeroelastic optimization of a 10 mw wind turbine blade with active trailing edge flaps. *AIAA*, 2016. doi: https://doi.org/10.2514/6.2016-1262.

List of Tables

List of Figures

A

MATLAB code: mathematical model

Below is a condensed version of the file to understand the structure. The files that were used contain more options and are available on request and will be sent to the supervisors. The used files can: tune the pre-load, sort results, use different time integration methods and create a table of results.

```
clearvars -except Mp_tune coef CL;
%% ======================< Semi-Passive flap >============================
% By: Jesse La Porte
% Date:  20/03/19
% Input:
%       * aoa
%       * Vrel
%       * delta  (flap angle)
%       * span
% CASE: Kf   mom dom c_f span
% For running a single case when the mpre-loads are know, or the pre-loads
% can be tuned manually by checking the output in the cmd window.
%% ============================< Input >=================================
rho     = 1.225;          % density of air
dt      = 0.01;           % time step, equal to HAWC2
time    = 0:dt:100;       % total time signal
mb      = 1.6874e+03;     % Mass of blade sectio for 10% span
R       = 86.3660;        % [m] total radius
coef.c10.re10  = xlsread('re10e6_chord10.xlsx'); % chord = 10 re10e6
coef.c10.re12  = xlsread('re12e6_chord10.xlsx'); % chord = 10 re12e6

% this file does not tune the pre-load... input below:
MP = [0,0,0,0,0,0 ... kf[50-150], omper[.3] doff=0.1
0,0,20,-60,30,60]; % chord.10 span 10

% Parameters
Kf      = 40;             % [Nm/deg]
mom     = 0.30*mb;        % [kg] % of mb.
dom     = 0.1*3.2528;     % [m] 1% chord
c_f     = 0.1*3.2528;     % [m] 10% chord
span    = 0.1*R;          % [m] 10% span
fn      = 1/(2*pi)*sqrt(Kf/mom);

Jf      = dom^2*mom;      % Flap inertia
% Read HAWC2 statistics, saved in function
[aoa,VR,rot_x,rot_y,rot_z,a_max,Bmu,F] = HAWC2_baseline();

% To save variables
D0 = zeros(length(time),12); DDD0 = zeros(length(time),12); ACC2 = zeros(length(time),12);
MI = zeros(length(time),12); DD0  = zeros(length(time),12); ARM1 = zeros(length(time),12);
MA = zeros(length(time),12); ACC1 = zeros(length(time),12); ARM2 = zeros(length(time),12);
for i    = 1:12 % windspeed
d0      = 0;  d0_dot  = 0;  d0_ddot = 0; STOP = 0;
if i < 5  % read hinge coeff data for below rated
CL.a    = coef.c10.re10(2:end,1);
```

```
CL.d    = coef.c10.re10(1,2:end);
CL.CL   = coef.c10.re10(2:end,2:end);
else     % read hinge coeff data for above rated
CL.a    = coef.c10.re12(2:end,1);
CL.d    = coef.c10.re12(1,2:end);
CL.CL   = coef.c10.re12(2:end,2:end);
end
%[A_max] = RH_rotation(rot_x(i),rot_y(i),rot_z(i),a_max(i,:));
% rotation matrices written out
A_maxx = a_max(i,1)*cosd(rot_z(i))*cosd(rot_y(i)) + a_max(i,2)*sind(rot_z(i))*cosd(rot_y(i)) - a_max(i,3)*
A_maxy = a_max(i,1)*(-sind(rot_z(i))*cosd(rot_x(i))+cosd(rot_z(i))*sind(rot_y(i))*sind(rot_x(i))) + a_max(
alfa    = aoa(i);
Vrel    = VR(i,2);
f       = F(i);                                  % [Hz] 1P frequency

for q   = 1:length(time)
t       =  time(q);
acc     = [A_maxx*sin(2*pi*f*t)+Bmu(1,i); A_maxy*cos(2*pi*f*t)+Bmu(2,i)]; % Time varying acceleration
C_H     = interp2(CL.d,CL.a,CL.CL,d0,alfa); % bilinear interpolation

%% ============================< Equations of motion >====================
% Time Marching
Ma      = -0.5*rho*span*c_f^2*C_H*Vrel^2;
Mi      = -dom*mom*(cosd(d0)*acc(2)- sind(d0)*acc(1));
Mp      = MP(i);

d0_ddot = -Kf*d0/Jf + (Ma +Mi+ Mp)/Jf;  % instant

% Euler-Cromer, stable for oscillating problems
d1_dot  = d0_dot + d0_ddot*dt;              % next velocity
d0      = d0 +d1_dot*dt;                    % next position
d0_dot  = d1_dot;
% Mechanical stop
if d0 >= 10
d0 =10;
d0_dot=0;
STOP = 1;
elseif d0 <= -10
d0 = -10;
d0_dot=0;
STOP = 1;
else
end
% Create vectors of data
D0(q,i)       = d0;
DDD0(q,i)= d0_ddot; DD0(q,i) = d0_dot;%ARM1(q,i) = arm(1);ARM2(q,i)     = arm(2);
MI(q,i)       = Mi;
MA(q,i)  = Ma; ACC1(q,i) = acc(1); ACC2(q,i) = acc(2);
end
%% ============================< Output >=================================
MEAN(i,1)    = mean(D0(:,i));
fprintf('Wsp = %d, mean = %0.3f [deg] Mp = %0.3f [deg], STOP = %d\n',i, MEAN(i),Mp,STOP)
end
figure();%yyaxis right;yyaxis left;
%plot(MI(:,3)); ylabel('MI');
plot(ACC1(:,3)); hold on;plot(ACC2(:,3));
plot(D0(:,3));legend('acc_x','acc_y','flap');%
xlabel('Time [s]')
ylabel('Flap deflection')
nicefig; set(gca,'FontSize', 11)
```

B

Fortran code: .dll

```
module passive_flap_ctrl_mod
implicit none
!   Declare all variables we are in Fortran   !
real*8 rho                ! air density [kg/m^3]
real*8 Jf                 ! flap inertia [kgm^2]
real*8 mb                 ! blade section mass [kg]
real*8 Kf                 ! flap stiffness [Nm/deg]
real*8 Mp                 ! pre-load [Nm]
real*8 mom                ! offset mass percentage [%]
real*8 dom                ! offset mass distance percentage [%]
real*8 c                  ! aerofoil chord at mid-flap postion [m]
real*8 c_f                ! flap chord at mid-flap postion [%]
real*8 dr_f               ! flap spanwise length [m]
real*8 time               ! simulation time [s]
real*8 aoa1                ! angle of attack at mid-flap position [deg]
real*8 aoa2                ! angle of attack at mid-flap position [deg]
real*8 aoa3                ! angle of attack at mid-flap position [deg]
real*8 vrel1               ! relative velocity at mid-flap position on blade 1[m/s]
real*8 vrel2               ! relative velocity at mid-flap position on blade 2[m/s]
real*8 vrel3               ! relative velocity at mid-flap position on blade 3[m/s]
real*8 acc1_x              ! acceleration at flap hinge at mid-flap position on blade 1[m/s^2]
real*8 acc1_y              ! acceleration at flap hinge at mid-flap position on blade 1[m/s^2]
real*8 acc1_z              ! acceleration at flap hinge at mid-flap position on blade 1[m/s^2]
real*8 acc2_x              ! acceleration at flap hinge at mid-flap position on blade 2[m/s^2]
real*8 acc2_y              ! acceleration at flap hinge at mid-flap position on blade 2[m/s^2]
real*8 acc2_z              ! acceleration at flap hinge at mid-flap position on blade 2[m/s^2]
real*8 acc3_x              ! acceleration at flap hinge at mid-flap position on blade 3[m/s^2]
real*8 acc3_y              ! acceleration at flap hinge at mid-flap position on blade 3[m/s^2]
real*8 acc3_z              ! acceleration at flap hinge at mid-flap position on blade 3[m/s^2]
real*8 eulerang1_x         ! rotation of mid flap blade1 section w.r.t blade root [deg]
real*8 eulerang1_y         ! rotation of mid flap blade1 section w.r.t blade root [deg]
real*8 eulerang1_z         ! rotation of mid flap blade1 section w.r.t blade root [deg]
real*8 eulerang2_x         ! rotation of mid flap blade2 section w.r.t blade root [deg]
real*8 eulerang2_y         ! rotation of mid flap blade2 section w.r.t blade root [deg]
real*8 eulerang2_z         ! rotation of mid flap blade2 section w.r.t blade root [deg]
real*8 eulerang3_x         ! rotation of mid flap blade3 section w.r.t blade root [deg]
real*8 eulerang3_y         ! rotation of mid flap blade3 section w.r.t blade root [deg]
real*8 eulerang3_z         ! rotation of mid flap blade3 section w.r.t blade root [deg]
real*8 beta_ref_1_1_old    ! flap angle of flap 1 on blade 1 - previous time step [deg]
real*8 beta_ref_2_1_old    ! flap angle of flap 1 on blade 2 - previous time step [deg]
real*8 beta_ref_3_1_old    ! flap angle of flap 1 on blade 3 - previous time step [deg]
real*8 beta_ref_1_1        ! flap angle of flap 1 on blade 1 [deg]
real*8 beta_ref_2_1        ! flap angle of flap 1 on blade 2 [deg]
real*8 beta_ref_3_1        ! flap angle of flap 1 on blade 3 [deg]
real*8 beta1_ddot          ! flap acceleration blade 1[m/s2]
real*8 beta2_ddot          ! flap acceleration blade 2[m/s2]
real*8 beta3_ddot          ! flap acceleration blade 3[m/s2]
real*8 beta1_dot           ! flap velocity blade 1[m/s2]
```

```
real*8 beta2_dot           ! flap velocity blade 2[m/s2]
real*8 beta3_dot           ! flap velocity blade 3[m/s2]
real*8 ab1x                ! blade acceleration in blade1 section coor. x-direction [m/s2]
real*8 ab1y                ! blade acceleration in blade1 section coor. y-direction [m/s2]
real*8 ab2x                ! blade acceleration in blade2 section coor. x-direction [m/s2]
real*8 ab2y                ! blade acceleration in blade2 section coor. y-direction [m/s2]
real*8 ab3x                ! blade acceleration in blade3 section coor. x-direction [m/s2]
real*8 ab3y                ! blade acceleration in blade3 section coor. y-direction [m/s2]
real*8 Mi1                 ! Inertial moment blade 1
real*8 Mi2                 ! Inertial moment blade 2
real*8 Mi3                 ! Inertial moment blade 3
real*8 Ma1                 ! Aerodynamic moment blade 1
real*8 Ma2                 ! Aerodynamic moment blade 2
real*8 Ma3                 ! Aerodynamic moment blade 3
real*8 CH1                 ! Aerodynamic moment blade 1
real*8 CH2                 ! Aerodynamic moment blade 2
real*8 CH3                 ! Aerodynamic moment blade 3
real*8 AoaStart            ! AOASTART
real*8 BetaStart           !
real*8 NumsBeta            !
real*8 A10                ! aoa0 for interpolation
real*8 A11                ! aoa1 for interpolation
real*8 B10               ! beta0 for interpolation
real*8 B11               ! beta1 for interpolation
real*8 index11              ! index1 for interpolation
real*8 index12              ! index2 for interpolation
real*8 index13              ! index3 for interpolation
real*8 index14              ! index4 for interpolation
real*8 f10
real*8 f11
real*8 A0                ! aoa0 for interpolation
real*8 A1                ! aoa1 for interpolation
real*8 B0               ! beta0 for interpolation
real*8 B1               ! beta1 for interpolation
real*8 index1              ! index1 for interpolation
real*8 index2              ! index2 for interpolation
real*8 index3              ! index3 for interpolation
real*8 index4              ! index4 for interpolation
real*8, allocatable :: cdata3(:,:) ! read in the hinge coeff data.
real*8, allocatable :: cdata(:,:) ! Ch below rated
real*8, allocatable :: cdata2(:,:) ! Ch above rated
real*8 f0
real*8 f1
integer i
integer n
integer j
real*8 wsp
!
contains
!%%%%%%%%%%%%%%%%%%%%%%%%%%%%%%%%%%%%%%%%%%%%%%%%%%%%%%%%%%%%%%%%%%%%%%%%%%%%%%%%%%%%%%%%%%%%%%%%%%%%%%%%%%
! ----------------------------- Initialization SubRoutine ---------------------------------
subroutine init_passive_flap_ctrl(array1,array2)
implicit none
!DEC$ ATTRIBUTES DLLEXPORT, C, ALIAS:'init_passive_flap_ctrl' :: init_passive_flap_ctrl
real*8 array1(9) ! Input array, from hawc2 to dll
real*8 array2(1)  ! Array dll -> hawc2 In this case dummy 0
! - Read in parameters -
rho = array1(1)
mb = array1(2)
c = array1(3)
dr_f = array1(4)
mom  = array1(5)
dom  = array1(6)
c_f  = array1(7)
Kf   = array1(8)
wsp = array1(9)
! Initialize flap velocities as zero
beta1_dot = 0
beta2_dot = 0
beta3_dot = 0
! For reading the data
```

```
AoaStart    = -5            !
BetaStart   = -10           !
NumsBeta    = 21            !
Jf          = dom**2*c**2*mom*mb
IF (wsp== 4)THEN ! 1
mp = -17 !
ELSE IF (wsp== 6) THEN ! 7
mp = -8   !
ELSE IF (wsp== 8) THEN ! 13
mp = 0 !
ELSE IF (wsp== 10) THEN ! 19
mp = 24 !
ELSE IF (wsp== 12) THEN ! 25
mp = 50 !
ELSE IF (wsp== 14) THEN ! 31
mp = 13 !
ELSE IF (wsp== 16) THEN ! 37
mp = -7!
ELSE IF (wsp== 18) THEN ! 43
mp = -22 !
ELSE IF (wsp== 20) THEN ! 49
mp = -35 !
ELSE IF (wsp== 22) THEN ! 55
mp = -50 !
ELSE IF (wsp== 24) THEN ! 61
mp = -90 !
ELSE IF (wsp== 26) THEN ! 67
mp = -65!
END IF
!
    open(11,file='./control/CHdata.dat')
    n = 441
    read(11,*,end=1)
1     rewind(11)
    allocate(cdata(n,3))
    do i = 1, n
        read(11,*) cdata(i,:)
    end do
        close(11)
   cdata = transpose(cdata)
!
    open(12,file='./control/CHdata2.dat')
    read(12,*,end=1)
2    rewind(12)
    allocate(cdata2(n,3))
    do i = 1, n
    read(12,*) cdata2(i,:)
    end do
    close(12)
    cdata2 = transpose(cdata2)
!
! dummy output to HAWC2 *dont understand this..*
array2(1) = 1.d0 !tkba
!
end subroutine init_passive_flap_ctrl
! ------------------------------------------------------------------------------ !
! ----------------------------- Update SubRoutine ------------------------------ !
! ------------------------------------------------------------------------------ !
subroutine update_passive_flap_ctrl(array1,array2)
implicit none
!DEC$ ATTRIBUTES DLLEXPORT, C, ALIAS:'update_passive_flap_ctrl' :: update_passive_flap_ctrl
real(8) array1(31)  ! Input array, from hawc2 to dll
real(8) array2(6)   ! Array dll -> hawc2
! Read flap data
if (wsp <= 10) then
    cdata3 = cdata
elseif (wsp > 10) then
    cdata3 = cdata2
end if
! ------------------------------------------------------------------- !
! ------------------------- Main Body --------------------------- !
```

```
! ------------------------------------------------------------- !
!--- Read Input vector ---- !
time = array1(1)
aoa1 = array1(2)
aoa2 = array1(3)
aoa3 = array1(4)
vrel1 = array1(5)
vrel2 = array1(6)
vrel3 = array1(7)
acc1_x = array1(8)      !
acc1_y = array1(9)      !
acc1_z = array1(10)     !
acc2_x = array1(11)     !
acc2_y = array1(12)     !
acc2_z = array1(13)     !
acc3_x = array1(14)     !
acc3_y = array1(15)     !
acc3_z = array1(16)     !
beta_ref_1_1_old = array1(17)
beta_ref_2_1_old = array1(18)
beta_ref_3_1_old = array1(19)
eulerang1_x = array1(20)
eulerang1_y = array1(21)
eulerang1_z = array1(22)
eulerang2_x = array1(23)
eulerang2_y = array1(24)
eulerang2_z = array1(25)
eulerang3_x = array1(26)
eulerang3_y = array1(27)
eulerang3_z = array1(28)
beta1_dot = array1(29)
beta2_dot = array1(30)
beta3_dot = array1(31)
!--- Start flap modelling here --- !
! ================================================================== !
! ================================== Flap 1 ========================== !
! ================================================================== !
! Rotate accelerations !
ab1x = (acc1_x*cosd(eulerang1_z)*cosd(eulerang1_y) + acc1_y*sind(eulerang1_z)*cosd(eulerang1_y) - acc1_z*s
ab1y = (acc1_x*(-sind(eulerang1_z)*cosd(eulerang1_x)+cosd(eulerang1_z)*sind(eulerang1_y)*sind(eulerang1_x)
! calculate inertial moment    Mi = r X ma
Mi1     = -dom*c*mb*mom*(COSD(beta_ref_1_1_old)*ab1y-SIND(beta_ref_1_1_old)*ab1x)
! Aerodyanmic Moment
A0 = int(aoa1 - DBLE(AoaStart))
A1 = int(aoa1 - DBLE(AoaStart-1))
B0 = int(beta_ref_1_1_old - DBLE(BetaStart -1))
B1 = int(beta_ref_1_1_old - DBLE(BetaStart -2))
! GET THE NEARBY INDICES OF THE
index1 = min(n,int(max(1d0,A0*DBLE(NumsBeta)+B0)))
index2 = min(n,int(max(1d0,A0*DBLE(NumsBeta)+B1)))
index3 = min(n,int(max(1d0,A1*DBLE(NumsBeta)+B0)))
index4 = min(n,int(max(1d0,A1*DBLE(NumsBeta)+B1)))
!
f0 = (A1 + DBLE(AoaStart) - aoa1)
f1 = (B1 + DBLE(BetaStart-1) - beta_ref_1_1_old)
CH1    = (cdata3(3,index1)*f1   + cdata3(3,index2)*(1-f1))*f0 + (cdata3(3,index3)*f1   +cdata3(3,index4)*(
Ma1     = -0.5*rho*c_f**2*c**2*vrel1**2*dr_f*CH1
!print *, 'Mi = ', Mi1
!print *, 'Ma = ', Ma1
! Solve for flap acceleration
beta1_ddot = -Kf*beta_ref_1_1_old/Jf + (Ma1 + Mi1 + Mp)/Jf
! March velocity forwards Euler-Cromer algorithm
beta1_dot  = beta1_dot+beta1_ddot*0.01

! March position forward: Euler-Cromer Algorithm
beta_ref_1_1   = beta_ref_1_1_old +beta1_dot*0.01
!print *, 'ddot = ', beta1_ddot
!print *, 'dot = ', beta1_dot
print *, 'd = ', beta_ref_1_1_old
! Mechanical stop.
IF (beta_ref_1_1 >= 10) THEN
```

```
   beta_ref_1_1 = 10
   beta1_dot    = 0
   beta1_ddot = 0
ELSE IF (beta_ref_1_1 <= -10) THEN
   beta_ref_1_1 = -10
   beta1_dot    = 0
   beta1_ddot   = 0
ELSE
END IF
! ================================================================== !
! ================================== Flap 2 ======================== !
! ================================================================== !
ab2x = (acc2_x*cosd(eulerang2_z)*cosd(eulerang2_y) + acc2_y*sind(eulerang2_z)*cosd(eulerang2_y) - acc2_z*sind(eu
ab2y = (acc2_x*(-sind(eulerang2_z)*cosd(eulerang2_x)+cosd(eulerang2_z)*sind(eulerang2_y)*sind(eulerang2_x)) + ac
! Calculate inertial moment    Mi = r X ma
Mi2     = -dom*c*mb*mom*(COSD(beta_ref_2_1_old)*ab2y-SIND(beta_ref_2_1_old)*ab2x)
! Aerodynamic moment 2
A0 = int(aoa2 - DBLE(AoaStart))
A1 = int(aoa2 - DBLE(AoaStart-1))
B0 = int(beta_ref_2_1_old - DBLE(BetaStart -1))
B1 = int(beta_ref_2_1_old - DBLE(BetaStart -2))
! GET THE TO NEARBY INDICES OF THE
index1 = min(n,int(max(1d0,A0*DBLE(NumsBeta)+B0)))
index2 = min(n,int(max(1d0,A0*DBLE(NumsBeta)+B1)))
index3 = min(n,int(max(1d0,A1*DBLE(NumsBeta)+B0)))
index4 = min(n,int(max(1d0,A1*DBLE(NumsBeta)+B1)))
!
f0 = (A1 + DBLE(AoaStart) - aoa2)
f1 = (B1 + DBLE(BetaStart-1) - beta_ref_2_1_old)
CH2     = (cdata3(3,index1)*f1   + cdata3(3,index2)*(1-f1))*f0 + (cdata3(3,index3)*f1   +cdata3(3,index4)*(1-f1))
Ma2     = -0.5*rho*c_f**2*c**2*vrel2**2*dr_f*CH2
! Solve for flap acceleration
beta2_ddot = -Kf*beta_ref_2_1_old/Jf + (Ma2 + Mi2 + Mp)/Jf
! March velocity forwards Euler-Cromer algorithm
beta2_dot  = beta2_dot+beta2_ddot*0.01
! March position forward: Euler-Cromer Algorithm
beta_ref_2_1   = beta_ref_2_1_old +beta2_dot*0.01
! Mechanical stop.
IF (beta_ref_2_1 >= 10) THEN
   beta_ref_2_1 = 10
   beta2_dot    = 0
      beta2_ddot = 0
ELSE IF (beta_ref_2_1 <= -10) THEN
   beta_ref_2_1 = -10
   beta2_dot    = 0
   beta2_ddot = 0
ELSE
END IF
! ================================================================== !
! ================================== Flap 3 ======================== !
! ================================================================== !
ab3x = (acc3_x*cosd(eulerang3_z)*cosd(eulerang3_y) + acc3_y*sind(eulerang3_z)*cosd(eulerang3_y) - acc3_z*sind(eu
ab3y = (acc3_x*(-sind(eulerang3_z)*cosd(eulerang3_x)+cosd(eulerang3_z)*sind(eulerang3_y)*sind(eulerang3_x)) + ac
! calculate inertial moment    Mi = r X ma
Mi3     = -dom*c*mb*mom*(COSD(beta_ref_3_1_old)*ab1y-SIND(beta_ref_3_1_old)*ab3x)
! Aerodynamic moment 2
A0 = int(aoa3 - DBLE(AoaStart))
A1 = int(aoa3 - DBLE(AoaStart-1))
B0 = int(beta_ref_3_1_old - DBLE(BetaStart -1))
B1 = int(beta_ref_3_1_old - DBLE(BetaStart -2))
! GET THE TO NEARBY INDICES OF THE
index1 = min(n,int(max(1d0,A0*DBLE(NumsBeta)+B0)))
index2 = min(n,int(max(1d0,A0*DBLE(NumsBeta)+B1)))
index3 = min(n,int(max(1d0,A1*DBLE(NumsBeta)+B0)))
index4 = min(n,int(max(1d0,A1*DBLE(NumsBeta)+B1)))
!
f0 = (A1 + DBLE(AoaStart) - aoa3)
f1 = (B1 + DBLE(BetaStart-1) - beta_ref_3_1_old)
CH3     = (cdata3(3,index1)*f1   + cdata3(3,index2)*(1-f1))*f0 + (cdata3(3,index3)*f1   +cdata3(3,index4)*(1-f1))
Ma3     = -0.5*rho*c_f**2*c**2*vrel3**2*dr_f*CH3
! Solve for flap acceleration
```

```
beta3_ddot = -Kf*beta_ref_3_1_old/Jf + (Ma3 + Mi3 + Mp)/Jf
! March velocity forwards Euler-Cromer algorithm
beta3_dot  = beta3_dot+beta3_ddot*0.01
! March position forward: Euler-Cromer Algorithm
beta_ref_3_1   = beta_ref_3_1_old +beta3_dot*0.01
!
! Mechanical stop.
IF (beta_ref_3_1 >= 10) THEN
   beta_ref_3_1 = 10
   beta3_dot    = 0
   beta3_ddot = 0
ELSE IF (beta_ref_3_1 <= -10) THEN
   beta_ref_3_1 = -10
   beta3_dot    = 0
   beta3_ddot = 0
ELSE
END IF
! ------------------------------------------------------------- !
! =================== Output to HAWC2 ========================== !
! ------------------------------------------------------------- !
! Flap control actions
array2(1)  = beta_ref_1_1
array2(2)  = beta_ref_2_1
array2(3)  = beta_ref_3_1
array2(4)  = beta1_dot
array2(5)  = beta2_dot
array2(6)  = beta3_dot
!
end subroutine update_passive_flap_ctrl
!**************************************************************************************************
end module passive_flap_ctrl_mod
```

C

Additional tables

Table C.1: Table from Pdap, listing the ultimate loads for each signal and from which dlc it originates, for the baseline.

Name	Min incl. psd	Max incl. psd	DLC min	DLC max
MxTB	-5.47E+04	2.93E+05	12_wsp04_wdir350_s1001	12_wsp12_wdir010_s6005
MyTB	-9.17E+04	1.38E+05	12_wsp26_wdir350_s2012	12_wsp26_wdir000_s3012
MxTT	-4.19E+04	4.69E+04	12_wsp24_wdir350_s2011	12_wsp26_wdir010_s5012
MyTT	-6.40E+02	1.90E+04	12_wsp04_wdir000_s3001	12_wsp24_wdir010_s5011
MzTT	-4.80E+04	5.32E+04	12_wsp22_wdir010_s5010	12_wsp22_wdir350_s1010
MxMB	-4.48E+04	4.93E+04	12_wsp26_wdir350_s2012	12_wsp22_wdir350_s1010
MyMB	-5.04E+04	5.02E+04	12_wsp22_wdir010_s5010	12_wsp26_wdir350_s2012
MzMB	-1.98E+04	5.64E+01	12_wsp26_wdir350_s2012	12_wsp04_wdir350_s1001
MxBR	-5.31E+04	2.95E+04	12_wsp12_wdir010_s6005	12_wsp26_wdir010_s5012
MyBR	-2.07E+04	2.09E+04	12_wsp26_wdir000_s4012	12_wsp12_wdir010_s6005
MzBR	-7.35E+02	6.01E+02	12_wsp24_wdir010_s6011	12_wsp12_wdir010_s6005
TTDist	8.87E+00	9.57E+01	12_wsp12_wdir000_s3005	12_wsp26_wdir000_s4012

Table C.2: Table from Pdap, listing the ultimate loads for each signal and from which dlc it originates, for the 10% flap.

Name	Min incl. psd	Max incl. psd	DLC min	DLC max
MxTB	-6.09E+04	2.82E+05	12_wsp04_wdir350_s1001	12_wsp12_wdir010_s6005
MyTB	-9.93E+04	1.31E+05	12_wsp26_wdir350_s2012	12_wsp24_wdir010_s5011
MxTT	-4.30E+04	4.60E+04	12_wsp26_wdir000_s3012	12_wsp26_wdir000_s4012
MyTT	-6.49E+02	1.90E+04	12_wsp04_wdir000_s3001	12_wsp26_wdir000_s4012
MzTT	-4.84E+04	5.13E+04	12_wsp26_wdir000_s4012	12_wsp26_wdir350_s2012
MxMB	-4.69E+04	4.86E+04	12_wsp26_wdir350_s2012	12_wsp22_wdir350_s1010
MyMB	-4.73E+04	4.80E+04	12_wsp22_wdir010_s5010	12_wsp26_wdir350_s2012
MzMB	-2.00E+04	5.83E+01	12_wsp26_wdir350_s2012	12_wsp04_wdir350_s1001
MxBR	-5.24E+04	2.85E+04	12_wsp12_wdir010_s6005	12_wsp26_wdir000_s4012
MyBR	-2.03E+04	2.05E+04	12_wsp26_wdir000_s3012	12_wsp12_wdir010_s6005
MzBR	-8.08E+02	5.80E+02	12_wsp24_wdir010_s6011	12_wsp12_wdir010_s6005
TTDist	8.82E+00	9.55E+01	12_wsp12_wdir000_s3005	12_wsp22_wdir350_s1010

Table C.3: Table from Pdap, listing the ultimate loads for each signal and from which dlc it originates, for the 30% flap.

Name	Min incl. psd	Max incl. psd	DLC min	DLC max
MxTB	-6.50E+04	3.00E+05	12_wsp04_wdir000_s4001	12_wsp12_wdir000_s4005
MyTB	-8.52E+04	1.32E+05	12_wsp26_wdir350_s2012	12_wsp26_wdir010_s6012
MxTT	-4.35E+04	4.39E+04	12_wsp26_wdir000_s3012	12_wsp24_wdir010_s6011
MyTT	-6.29E+02	1.92E+04	12_wsp04_wdir000_s3001	12_wsp24_wdir010_s5011
MzTT	-4.65E+04	4.73E+04	12_wsp24_wdir000_s4011	12_wsp26_wdir350_s2012
MxMB	-4.58E+04	4.15E+04	12_wsp26_wdir350_s2012	12_wsp24_wdir010_s5011
MyMB	-4.38E+04	4.87E+04	12_wsp26_wdir000_s4012	12_wsp26_wdir000_s3012
MzMB	-1.74E+04	4.64E+01	12_wsp26_wdir350_s2012	12_wsp04_wdir000_s3001
MxBR	-4.99E+04	2.90E+04	12_wsp12_wdir010_s6005	12_wsp26_wdir000_s4012
MyBR	-2.12E+04	2.02E+04	12_wsp26_wdir000_s4012	12_wsp12_wdir010_s6005
MzBR	-8.44E+02	5.73E+02	12_wsp24_wdir010_s6011	12_wsp12_wdir010_s6005
TTDist	9.15E+00	9.56E+01	12_wsp12_wdir010_s6005	12_wsp26_wdir350_s2012